



The *Hubble Space Telescope* UV Legacy Survey of Galactic globular clusters – XIII. ACS/WFC parallel-field catalogues

M. Simioni,^{1,2,3,4*} L. R. Bedin,⁴ A. Aparicio,^{1,2} G. Piotto,^{3,4} A. P. Milone,^{3,5} D. Nardiello,^{3,4} J. Anderson,⁶ A. Bellini,⁶ T. M. Brown,⁶ S. Cassisi,^{1,7} A. Cunial,³ V. Granata,^{3,4} S. Ortolani,^{3,4} R. P. van der Marel^{6,8} and E. Vesperini⁹

¹Instituto de Astrofísica de Canarias, E-38200 La Laguna, Tenerife, Canary Islands, Spain

²Department of Astrophysics, University of La Laguna, E-38200 La Laguna, Tenerife, Canary Islands, Spain

³Dipartimento di Fisica e Astronomia ‘Galileo Galilei’, Università degli Studi di Padova, Vicolo dell’Osservatorio 3, I-35122 Padova, Italy

⁴INAF – Osservatorio Astronomico di Padova, Vicolo dell’Osservatorio 5, I-35122 Padova, Italy

⁵Research School of Astronomy and Astrophysics, Australian National University, Cotter Road, Weston, ACT 2611, Australia

⁶Space Telescope Science Institute, 3700 San Martin Dr, Baltimore, MD 21218, USA

⁷INAF – Osservatorio Astronomico di Teramo, Via M. Maggini, I-64100 Teramo, Italy

⁸Center for Astrophysical Sciences, Department of Physics & Astronomy, Johns Hopkins University, Baltimore, MD 21218, USA

⁹Department of Astronomy, Indiana University, Bloomington, IN 47401, USA

Accepted 2018 January 17. Received 2018 January 17; in original form 2017 October 10

ABSTRACT

As part of the *Hubble Space Telescope* UV Legacy Survey of Galactic globular clusters, 110 parallel fields were observed with the Wide Field Channel of the Advanced Camera for Surveys, in the outskirts of 48 globular clusters, plus the open cluster NGC 6791. Totalling about 0.3 deg^2 of observed sky, this is the largest homogeneous *Hubble Space Telescope* photometric survey of Galactic globular clusters outskirts to date. In particular, two distinct pointings have been obtained for each target on average, all centred at about 6.5 arcmin from the cluster centre, thus covering a mean area of about 23 arcmin 2 for each globular cluster. For each field, at least one exposure in both $F475W$ and $F814W$ filters was collected. In this work, we publicly release the astrometric and photometric catalogues and the astrometrized atlases for each of these fields.

Key words: atlases – catalogues – Hertzsprung–Russell and colour–magnitude diagrams – globular clusters: general.

1 INTRODUCTION

For almost three decades, the Milky Way globular clusters (GCs) have been the target of large CCD photometric surveys aimed at sampling their stellar populations in a homogeneous way (Rosenberg, Piotto & Saviane 2000a, Rosenberg, Aparicio & Saviane 2000b, Piotto et al. 2002, Sarajedini et al. 2007) using both space- and ground-based instruments. The growing sample of data, and the advent of increasingly sophisticated data-analysis techniques, have clearly demonstrated that GCs host distinct stellar populations with different chemical abundances. High-precision photometric measurements have revealed that the colour–magnitude diagrams (CMDs) show distinct sequences in various evolutionary stages (see e.g. Anderson 1997, Lee et al. 1999; Pancino et al. 2000; Bedin et al. 2004; Piotto et al. 2007; Milone et al. 2008; Bellini et al. 2010). These findings are also supported by spectro-

scopical evidence that the stellar populations of these systems are not as simple as thought (see e.g. Kraft 1994; Gratton et al. 2004; Marino et al. 2008; Yong & Grundahl 2008; Carretta et al. 2009a; Carretta, Bragaglia & Gratton 2009b; Gratton et al. 2012).

The *Hubble Space Telescope* UV Legacy Survey of Galactic globular clusters (GO-13297; PI: Piotto) has been specifically designed to further investigate this phenomenon and it now appears likely that all Galactic GCs host multiple stellar populations (Piotto et al. 2015 – hereafter Paper I; Milone et al. 2017 – hereafter Paper IX). In the context of this survey, parallel Advanced Camera for Surveys (ACS) observations have been obtained. While the main observations were taken using a combination of UV and optical filters of the Wide Field Camera 3 (WFC3), the lack of filters bluer than $F435W$ dictated the use of the $F475W$ and $F814W$ filters of the Wide Field Channel of the ACS (ACS/WFC) in the parallel observations. The large colour baseline provided by this filter combination guarantees sensitivity to helium abundance differences, while being largely insensitive to star-to-star variations in light-element abundances (Sbordone, Salaris & Weiss 2011, Cassisi, Salaris & Pietrinferni 2017).

* E-mail: msimioni@iac.es (MS); luigi.bedin@oapd.inaf.it (LRB); aaj@iac.es (AA)

Table 1. Observation log. For each GC in the survey, and the open cluster NGC 6791, we show right ascension and declination of each distinct parallel field, referred to the centre of ACS/WFC. We also report the number of orbits, telescope orientation (V3 PA) for each orbit, and exposure time in each filter.

#	Cluster	Orbits	Field [PA (deg)]	RA (J2000) ($^h m s$)	Dec. (J2000) ($^{\circ} ' ''$)	Epoch	Exp. time <i>F475W</i> (s)	Exp. time <i>F814W</i> (s)
01	NGC 1261	5	F1 [92]	03:12:49.68	-55:17:25.2	31/08/13	770	694
			F2 [138]	03:12:16.96	-55:19:29.6	11/09/13	745	669
			F3 [182]	03:11:44.35	-55:17:39.3	08/11/13	766	690
			F4 [225]	03:11:30.53	-55:13:17.9	07/12/13	745	669
			F5 [48]	03:13:01.92	-55:12:51.4	29/06/14	829	753
02	NGC 1851	7	F1 [195]	05:13:37.57	-40:06:44.0	27/12/10	$2 \times 40; 2 \times 1277; 1237$	$6 \times 488; 1 \times 40$
			F2 [164]	05:13:51.57	-40:08:55.8	11/11/10	$2 \times 40; 2 \times 1277; 2 \times 1237$	$8 \times 488; 2 \times 40$
03	NGC 2298	4	F1 [185]	06:48:36.04	-36:05:08.7	18/12/13	2×785	2×683
			F2 [273]	06:48:35.14	-35:55:40.7	07/03/14	885	816
04	NGC 3201	2	F1 [25]	10:18:12.19	-46:21:47.1	13/09/13	685	612
			F2 [115]	10:17:54.00	-46:30:51.0	01/01/14	689	616
05	NGC 4590	2	F1 [112]	12:39:42.64	-26:50:34.9	21/12/13	627	554
			F2 [202]	12:39:01.10	-26:47:48.5	30/03/14	627	554
06	NGC 4833	4	F1 [113]	13:00:10.12	-70:58:29.4	17/01/14	2×840	2×771
			F2 [202]	12:58:20.68	-70:55:42.6	09/04/14	2×806	2×730
07	NGC 5024	6	F1 [31]	13:13:21.59	+18:12:01.1	24/03/14	$4 \times 725; 2 \times 723$	3×370
			F2 [120]	13:13:03.82	18:03:52.0	08/12/13	$4 \times 775; 2 \times 774$	3×375
08	NGC 5053	5	F1 [352]	13:16:42.03	+17:47:28.7	01/04/14	740	664
			F2 [37]	13:16:53.97	+17:43:15.0	16/03/14	740	664
			F3 [80]	13:16:50.28	+17:38:33.1	23/01/14	790	714
			F4 [125]	13:16:33.21	+17:35:39.5	05/12/13	790	714
			F5 [308]	13:16:21.88	+17:48:25.0	16/05/14	765	689
09	NGC 5286	2	F1 [73]	13:47:07.09	-51:25:00.2	14/12/13	728	655
			F2 [162]	13:46:11.09	-51:28:46.7	15/03/14	603	559
10	NGC 5466	4	F1 [112]	14:05:41.08	+28:26:12.1	05/01/14	$834; 835$	$763; 765$
			F2 [21]	14:05:54.29	+28:35:18.1	29/03/14	2×776	2×700
11	NGC 5897	4	F1 [112]	15:17:37.48	-21:06:27.5	12/02/14	$830; 833$	2×761
			F2 [202]	15:16:58.75	-21:03:44.3	13/05/14	$779; 781$	$710; 709$
12	NGC 5904	2	F1 [323]	15:18:34.23	02:11:38.3	17/05/14	620	559
			F2 [52]	15:19:00.34	02:04:36.4	08/04/14	621	559
13	NGC 5927	3	F1 [100]	15:28:28.73	-50:45:30.4	01/02/14	603	559
			F2 [189]	15:27:28.26	-50:44:48.7	19/05/14	603	559
14	NGC 5986	3	F1 [92]	15:46:28.87	-37:51:38.6	27/05/15	603	603
			F2 [180]	15:45:40.83	-37:52:21.9	17/05/14	603	559
						10/05/15	603	559
15	NGC 6093	5	F1 [255]	16:16:35.04	-22:55:45.9	09/06/12	$5 \times 760; 5 \times 845$	5×539
			F1 [147]	16:25:36.08	-72:18:35.2	04/04/14	762	686
			F2 [190]	16:24:40.57	-72:16:07.7	25/05/14	762	686
			F3 [235]	16:24:23.48	-72:11:18.6	29/06/14	800	724
			F4 [282]	16:24:58.26	-72:06:50.7	14/08/13	851	775
17	NGC 6121	2	F1 [272]	16:23:12.57	-26:27:02.1	06/07/14	739	666
			F2 [98]	16:23:55.64	-26:36:33.4	17/02/15	666	593
18	NGC 6144	2	F1 [83]	16:27:39.42	-26:05:00.9	28/02/14	679	606
			F2 [174]	16:26:57.33	-26:07:05.2	27/05/14	679	606
19	NGC 6171	4	F1 [342]	16:32:41.94	-12:56:56.1	31/05/14	$830; 833$	2×761
			F2 [72]	16:32:42.20	-12:57:07.5	25/03/14	$800; 802$	$731; 730$
20	NGC 6218	2	F1 [276]	16:46:55.21	-01:52:03.7	16/08/13	721	648
			F2 [6]	16:47:33.42	-01:52:07.7	27/05/14	645	572
21	NGC 6254	2	F1 [276]	16:56:50.04	-04:01:10.1	16/08/13	721	648
			F2 [7]	16:57:28.66	-04:01:19.2	27/05/14	644	571
22	NGC 6304	2	F1 [184]	17:14:10.53	-29:32:35.1	07/06/14	624	559
			F2 [274]	17:14:09.53	-29:23:04.8	26/08/13	731	658
23	NGC 6341	2	F1 [230]	17:16:30.21	+43:08:03.0	22/10/13	638	565
			F2 [319]	17:17:06.19	+43:14:56.0	03/08/14	750	677
24	NGC 6352	2	F1 [161]	17:25:15.00	-48:31:41.7	27/05/14	637	564
			F2 [251]	17:24:51.02	-48:22:52.5	13/08/13	731	658
25	NGC 6362	2	F1 [125]	17:32:14.07	-67:09:25.3	30/03/14	651	578
			F2 [215]	17:30:47.67	-67:04:37.3	01/07/14	760	687
26	NGC 6366	2	F1 [293]	17:27:31.94	-04:58:44.4	26/08/13	726	653

Table 1 – *continued*

#	Cluster	Orbits	Field [PA (deg)]	RA (J2000) ($^h m s$)	Dec. (J2000) ($^{\circ} '$ '')	Epoch	Exp. time <i>F475W</i> (s)	Exp. time <i>F814W</i> (s)
27	NGC 6388	4	F2 [351]	17:27:58.09	-04:58:57.1	07/06/15	644	571
			F1 [238]	17:35:40.80	-44:43:02.9	05/07/14	865; 906	796; 834
			F2 [141]	17:36:17.23	-44:50:53.5	12/05/14	793; 795	724; 723
28	NGC 6397	2	F1 [90]	17:41:17.47	-53:44:46.1	27/03/14	683	610
			F2 [180]	17:40:12.50	-53:45:38.3	11/06/14	640	567
29	NGC 6441	4	F1 [102]	17:50:34.23	-37:08:21.5	26/03/14	833; 835	764; 763
			F2 [192]	17:49:46.24	-37:07:12.6	15/06/14	2 × 794	725; 722
30	NGC 6496	2	F1 [157]	17:58:53.12	-44:22:28.2	30/05/14	638	656
			F2 [247]	17:58:27.50	-44:13:57.0	12/08/13	731	658
31	NGC 6535	2	F1 [319]	18:03:49.95	+00:11:04.6	19/07/14	724	651
			F2 [50]	18:04:17.63	+00:17:50.2	26/05/14	644	571
32	NGC 6541	2	F1 [80]	18:08:35.16	-43:46:11.5	14/02/14	689	616
			F2 [170]	18:07:44.04	-43:48:48.8	11/06/14	639	566
33	NGC 6584	2	F1 [155]	18:18:26.74	-52:19:31.3	30/05/14	640	567
			F2 [245]	18:17:54.89	-52:11:09.9	18/08/13	726	653
34	NGC 6624	2	F1 [264]	18:23:14.50	-30:17:51.1	03/09/13	731	658
			F2 [174]	18:23:23.29	-30:27:20.2	27/06/14	638	565
35	NGC 6637	4	F1 [84]	18:31:49.55	-32:24:40.9	18/02/14	827; 840	758; 768
			F2 [174]	18:31:05.49	-32:26:31.5	30/06/14	792; 794	723; 722
36	NGC 6652	3	F1 [281]	18:35:25.09	-32:54:08.8	30/08/13	707	633
			F2 [238]	18:35:14.87	-32:58:25.1	14/08/13	733	658
			F3 [192]	18:35:20.06	-33:03:36.1	01/07/14	621	548
37	NGC 6656	4	F1 [266]	18:36:00.25	-23:50:16.5	23/09/10	656; 644	2 × 389
			F2 [85]	18:36:47.76	-23:58:08.0	17/03/11	2 × 656	2 × 389
38	NGC 6681	2	F1 [271]	18:42:48.78	-32:13:03.7	05/09/13	730	658
			F2 [183]	18:42:51.19	-32:22:33.1	29/06/14	637	564
39	NGC 6715	6	F1 [153]	18:54:56.04	-30:35:08.9	29/06/14	2 × 736; 2 × 737; 2 × 734	3 × 370
			F2 [243]	18:54:33.96	-30:27:06.5	05/09/13	4 × 819; 2 × 817	3 × 390
40	NGC 6717	3	F1 [80]	18:55:31.98	-22:45:22.7	06/05/14	619	535
			F2 [125]	18:55:12.41	-22:48:27.0	03/07/14	619	544
			F3 [171]	18:54:51.25	-22:47:57.0	03/07/14	617	544
41	NGC 6723	3	F1 [103]	18:59:54.19	-36:43:18.0	03/04/14	666	592
			F2 [148]	18:59:27.49	-36:44:21.9	15/06/14	626	551
			F3 [193]	18:59:06.07	-36:41:59.9	05/07/14	624	551
42	NGC 6779	2	F1 [241]	19:16:04.77	+30:12:18.9	13/10/13	731	658
			F2 [333]	19:16:42.17	+30:17:38.2	19/07/14	637	564
43	NGC 6791	2	F1 [322]	19:20:53.69	+37:53:04.8	17/08/13	631	559
			F2 [50]	19:21:27.31	+37:46:16.6	26/04/14	638	565
44	NGC 6809	2	F1 [262]	19:39:32.79	-30:54:19.4	21/08/14	753	680
			F2 [82]	19:40:26.65	-31:01:26.4	29/03/14	677	604
45	NGC 6838	2	F1 [244]	19:53:18.63	+18:48:20.3	23/10/13	723	650
			F2 [75]	19:54:12.48	+18:43:53.9	03/05/14	681	608
46	NGC 6934	2	F1 [245]	20:33:44.84	+07:25:55.5	08/10/13	723	650
			F2 [334]	20:34:17.59	+07:30:52.3	18/08/14	644	571
47	NGC 6981	2	F1 [289]	20:53:13.45	-12:26:24.9	13/08/13	641	568
			F2 [19]	20:53:51.29	-12:28:39.5	03/08/14	624	551
48	NGC 7089	3	F1 [237]	21:32:59.85	+00:48:42.0	18/10/13	717	643
			F2 [281]	21:33:10.93	+00:44:15.0	29/08/13	668	593
			F3 [327]	21:33:29.92	+00:42:39.1	14/08/13	611	534
49	NGC 7099	2	F1 [92]	21:40:44.34	-23:15:15.1	08/06/14	656	583
			F2 [182]	21:40:02.30	-23:15:49.0	19/08/14	656	583

One of the main objectives for which these observations were planned is to investigate how different stellar populations formed in GCs. Strong observational constraints come from the analysis of the radial distribution of each stellar population (D’Ercole et al. 2008; Bellini et al. 2009; Vesperini, McMillan & D’Antona 2013). As an example, Simioni et al. (2016) complemented WFC3 data of the central regions of NGC 2808 with ACS parallel observations and found evidence of different radial trends associated with distinct stellar populations hosted by the cluster. Thus, clusters with large

helium variations among their stellar populations are the preferred target of investigation with the current data-sample. Other interesting targets, albeit extensively studied, are those defined as Type-II clusters in Paper IX, which displays multiple sub-giant branches in optical CMDs.

We stress the fact that this is the first homogeneous *HST* photometric survey of the outskirts of Galactic GCs. The observations presented here represent a first epoch for future studies aimed at systematical measurements of absolute, relative and internal proper

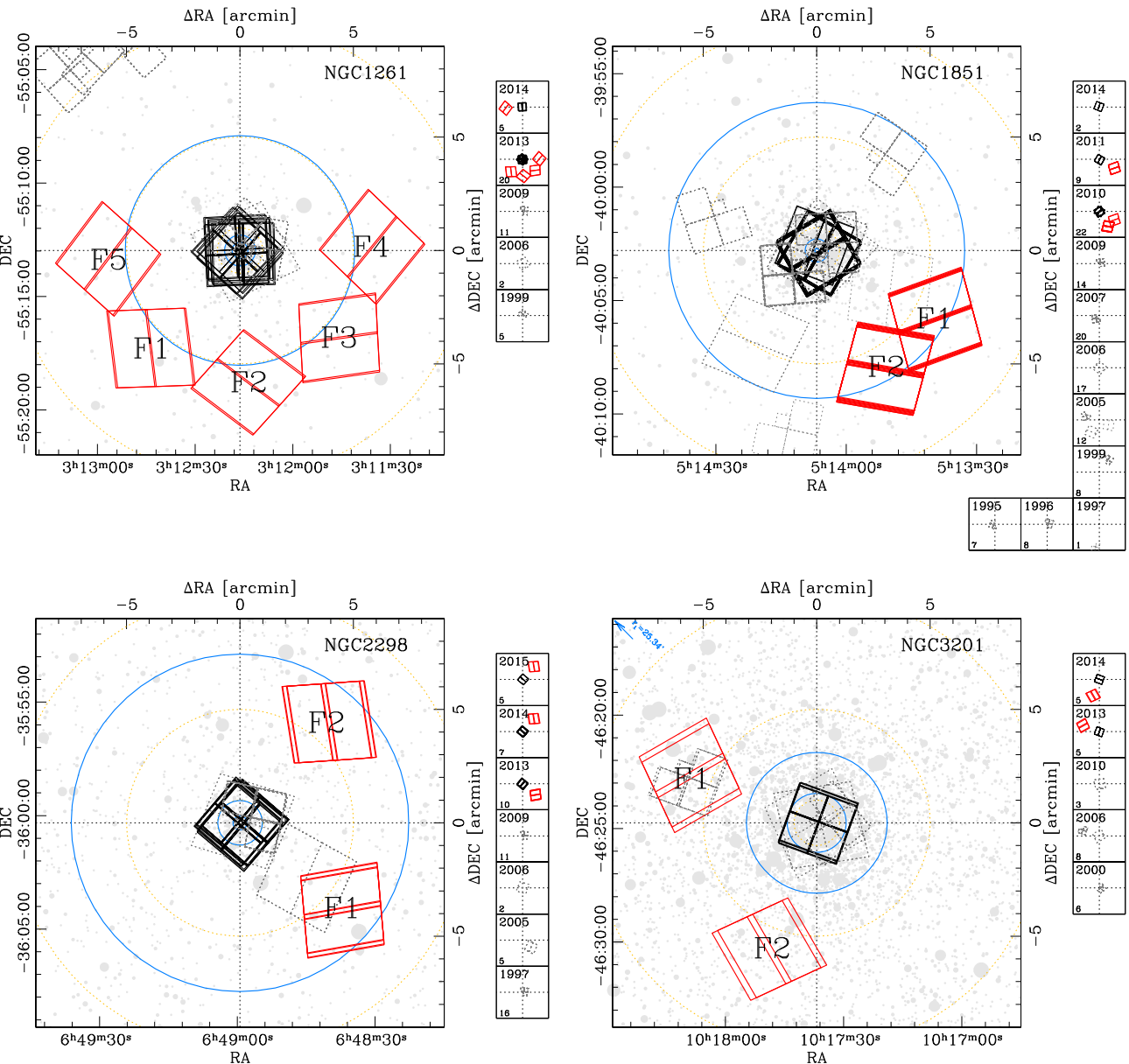


Figure 1. Finding charts for NGC 1261, NGC 1851, NGC 2298, and NGC 3201. Red outlines represent ACS/WFC parallel observations of GO-13297, black outlines refer to WFC3/UVIS observations. Dark grey, dashed outlines represent archive *HST* observations in the same regions. Footprints are labelled as in Table 1. Observations are subdivided by epoch in the smaller panels. Blue circles mark the position of core radius, half-light radius, and tidal radius for each cluster from Harris 1996 (2010). Where the tidal radius could not be included in the image, its value has been indicated in the upper-left corner of the image. Yellow, dashed circles mark the distances of 1, 5, and 10 arcmin from cluster centres. Grey dots correspond to 2MASS sources, with brighter sources being larger.

motions of stars in these regions. Archival *HST* observations matching a sub-sample of the observed fields exist, and proper motions will be published separately. In the imaged stellar fields, the stellar density is not as high as in the central regions. As a consequence, crowding is not a serious issue for these data. That makes them particularly suitable to be used as input catalogue for future spectroscopic surveys.

The present catalogues can be used to perform several interesting analyses. For example, dynamical interactions between stars in GCs is at the origin of the mass segregation phenomenon. A precise estimate of its effects is fundamental for the derivation of a global mass function for a GC (Vesperini & Heggie 1997; Paust et al. 2010; Sollima & Baumgardt 2017). The measurement of the fraction of

binaries is also fundamental for this kind of analysis and could provide useful constraints for dynamical models (Milone et al. 2012). We note, also, that in some cases white dwarf cooling sequences are visible in the obtained CMDs. Finally, it is interesting to note that due to the presence of many extragalactic objects in the observed field, other studies could benefit from these observations.

In this work, we present the first photometric catalogues from the ACS/WFC parallel observations of the GO-13297 program. All data have been reduced in a homogeneous manner, making these catalogues particularly suitable for intercomparison. The article is organized as follows: in Section 2 the data are presented along with some information about the observing strategy, together with a detailed description of the data reduction. The extracted CMDs are

Table 2. Tabulated $\Delta m_{\text{PSF-AP}(0.5 \text{ arcsec})}$ values used in the aperture correction.

#	Cluster	Field	$\Delta m_{\text{PSF-AP}(0.5 \text{ arcsec})}^{\text{F475W}}$ (mag)	$\Delta m_{\text{PSF-AP}(0.5 \text{ arcsec})}^{\text{F814W}}$ (mag)
01	NGC 1261	1	+0.016 ± 0.006	-0.017 ± 0.003
		2	+0.030 ± 0.005	-0.021 ± 0.002
		3	+0.021 ± 0.005	-0.013 ± 0.002
		4	+0.038 ± 0.005	+0.117 ± 0.005
		5	+0.053 ± 0.006	-0.020 ± 0.003
02	NGC 1851	1+2	-0.008 ± 0.002	-0.004 ± 0.001
03	NGC 2298	1	+0.057 ± 0.014	+0.148 ± 0.008
		2	+0.016 ± 0.010	+0.013 ± 0.005
04	NGC 3201	1	+0.022 ± 0.001	+0.001 ± 0.001
		2	+0.023 ± 0.001	+0.035 ± 0.001
05	NGC 4590	1	-0.003 ± 0.003	+0.002 ± 0.002
		2	0.000 ± 0.003	+0.039 ± 0.002
06	NGC 4833	1	+0.004 ± 0.002	+0.002 ± 0.001
		2	+0.009 ± 0.001	-0.008 ± 0.001
07	NGC 5024	1	+0.003 ± 0.001	+0.012 ± 0.001
		2	+0.009 ± 0.003	-0.019 ± 0.001
08	NGC 5053	1	+0.012 ± 0.004	+0.001 ± 0.004
		2	+0.003 ± 0.004	0.000 ± 0.003
		3	+0.005 ± 0.005	-0.011 ± 0.003
		4	+0.012 ± 0.005	+0.006 ± 0.003
		5	+0.132 ± 0.006	+0.029 ± 0.003
09	NGC 5286	1	+0.036 ± 0.003	+0.019 ± 0.002
		2	+0.031 ± 0.004	-0.011 ± 0.001
10	NGC 5466	1	+0.009 ± 0.003	-0.011 ± 0.003
		2	+0.008 ± 0.003	-0.009 ± 0.002
11	NGC 5897	1	+0.029 ± 0.003	-0.012 ± 0.001
		2	+0.028 ± 0.003	-0.014 ± 0.001
12	NGC 5904	1	+0.011 ± 0.001	-0.016 ± 0.001
		2	+0.003 ± 0.001	-0.008 ± 0.001
13	NGC 5927	1	+0.023 ± 0.002	+0.017 ± 0.001
		2	+0.022 ± 0.002	-0.003 ± 0.001
14	NGC 5986	1	-0.004 ± 0.002	-0.011 ± 0.001
		2	+0.043 ± 0.004	-0.008 ± 0.001
15	NGC 6093	1	+0.090 ± 0.002	+0.136 ± 0.002
16	NGC 6101	1	+0.003 ± 0.003	+0.004 ± 0.002
		2	+0.007 ± 0.003	-0.012 ± 0.001
		3	+0.010 ± 0.004	+0.004 ± 0.002
		4	+0.003 ± 0.002	-0.014 ± 0.001
		5	+0.009 ± 0.002	-0.001 ± 0.001
17	NGC 6121	1	+0.003 ± 0.002	+0.002 ± 0.001
		2	-0.004 ± 0.003	-0.005 ± 0.001
18	NGC 6144	1	+0.030 ± 0.004	+0.027 ± 0.001
		2	+0.013 ± 0.004	-0.002 ± 0.001
19	NGC 6171	1	+0.021 ± 0.002	-0.007 ± 0.002
		2	+0.022 ± 0.002	+0.004 ± 0.002
20	NGC 6218	1	-0.003 ± 0.002	-0.001 ± 0.001
		2	+0.006 ± 0.002	-0.009 ± 0.001
21	NGC 6254	1	-0.006 ± 0.002	+0.002 ± 0.001
		2	0.000 ± 0.002	-0.003 ± 0.001
22	NGC 6304	1	+0.010 ± 0.001	+0.036 ± 0.001
		2	+0.012 ± 0.002	+0.016 ± 0.001
23	NGC 6341	1	+0.003 ± 0.002	-0.026 ± 0.001
		2	+0.016 ± 0.002	-0.013 ± 0.001
24	NGC 6352	1	+0.001 ± 0.001	-0.004 ± 0.001
		2	-0.010 ± 0.001	+0.011 ± 0.001
25	NGC 6362	1	-0.002 ± 0.002	-0.006 ± 0.001
		2	+0.024 ± 0.003	+0.056 ± 0.001
26	NGC 6366	1	+0.023 ± 0.005	-0.003 ± 0.001
		2	+0.003 ± 0.002	+0.007 ± 0.001
27	NGC 6388	1	+0.011 ± 0.001	+0.016 ± 0.001
		2	+0.003 ± 0.001	+0.018 ± 0.001
28	NGC 6397	1	0.000 ± 0.001	+0.003 ± 0.001

Table 2 – continued

#	Cluster	Field	$\Delta m_{\text{PSF-AP}(0.5 \text{ arcsec})}^{\text{F475W}}$ (mag)	$\Delta m_{\text{PSF-AP}(0.5 \text{ arcsec})}^{\text{F814W}}$ (mag)
29	NGC 6441	2	+0.008 ± 0.002	+0.031 ± 0.001
		1	+0.010 ± 0.001	+0.027 ± 0.001
30	NGC 6496	2	+0.040 ± 0.001	+0.057 ± 0.001
		1	-0.008 ± 0.002	-0.005 ± 0.001
31	NGC 6535	2	-0.002 ± 0.002	+0.030 ± 0.001
		1	+0.010 ± 0.003	-0.007 ± 0.001
32	NGC 6541	2	0.000 ± 0.002	0.000 ± 0.001
		1	+0.011 ± 0.001	+0.020 ± 0.001
33	NGC 6584	2	-0.011 ± 0.003	-0.011 ± 0.001
		1	-0.005 ± 0.004	-0.016 ± 0.001
34	NGC 6624	2	+0.020 ± 0.001	+0.046 ± 0.001
		1	+0.008 ± 0.001	+0.014 ± 0.001
35	NGC 6637	2	+0.003 ± 0.001	+0.009 ± 0.001
		1	-0.008 ± 0.001	-0.003 ± 0.001
36	NGC 6652	2	-0.002 ± 0.002	+0.039 ± 0.001
		1	-0.008 ± 0.002	+0.003 ± 0.001
37	NGC 6656	3	+0.006 ± 0.001	+0.015 ± 0.001
		1	0.000 ± 0.001	+0.031 ± 0.001
38	NGC 6681	2	+0.079 ± 0.001	+0.030 ± 0.001
		1	-0.007 ± 0.001	-0.007 ± 0.001
39	NGC 6715	2	+0.001 ± 0.001	+0.033 ± 0.001
		1	+0.008 ± 0.001	+0.076 ± 0.001
40	NGC 6717	1	+0.006 ± 0.002	-0.013 ± 0.001
		2	-0.002 ± 0.002	+0.007 ± 0.001
41	NGC 6723	3	+0.005 ± 0.001	+0.011 ± 0.001
		1	-0.007 ± 0.003	0.000 ± 0.001
42	NGC 6779	2	+0.007 ± 0.002	-0.007 ± 0.001
		1	+0.016 ± 0.003	-0.008 ± 0.001
43	NGC 6791	2	+0.004 ± 0.003	0.000 ± 0.002
		1	-0.005 ± 0.002	+0.025 ± 0.002
44	NGC 6809	2	-0.005 ± 0.003	-0.011 ± 0.001
		1	+0.037 ± 0.002	-0.006 ± 0.001
45	NGC 6838	2	0.000 ± 0.001	-0.002 ± 0.001
		1	-0.014 ± 0.002	+0.016 ± 0.001
46	NGC 6934	2	+0.009 ± 0.002	-0.009 ± 0.001
		1	-0.001 ± 0.005	+0.004 ± 0.002
47	NGC 6981	2	+0.005 ± 0.007	-0.001 ± 0.003
		1	-0.002 ± 0.007	-0.009 ± 0.003
48	NGC 7089	2	+0.008 ± 0.011	+0.003 ± 0.005
		1	+0.014 ± 0.003	+0.016 ± 0.001
49	NGC 7099	2	+0.036 ± 0.002	-0.012 ± 0.001
		1	+0.003 ± 0.002	-0.020 ± 0.001

presented in Section 3. Details on the selection of well-measured stars are given in Section 4. In Section 5 the catalogues and the released electronic material are described in detail. Finally, in Section 6, after a summary, we briefly discuss some of the main scientific questions we will address with these catalogues in subsequent papers.

2 OBSERVATIONS AND DATA REDUCTION

Table reports the log of ACS/WFC observations used to construct the catalogues. For each target, we indicate the total number of orbits assigned to each observed field separated by the different position angles (PAs) of the V3 axis of the *HST* focal plane. Typically, one

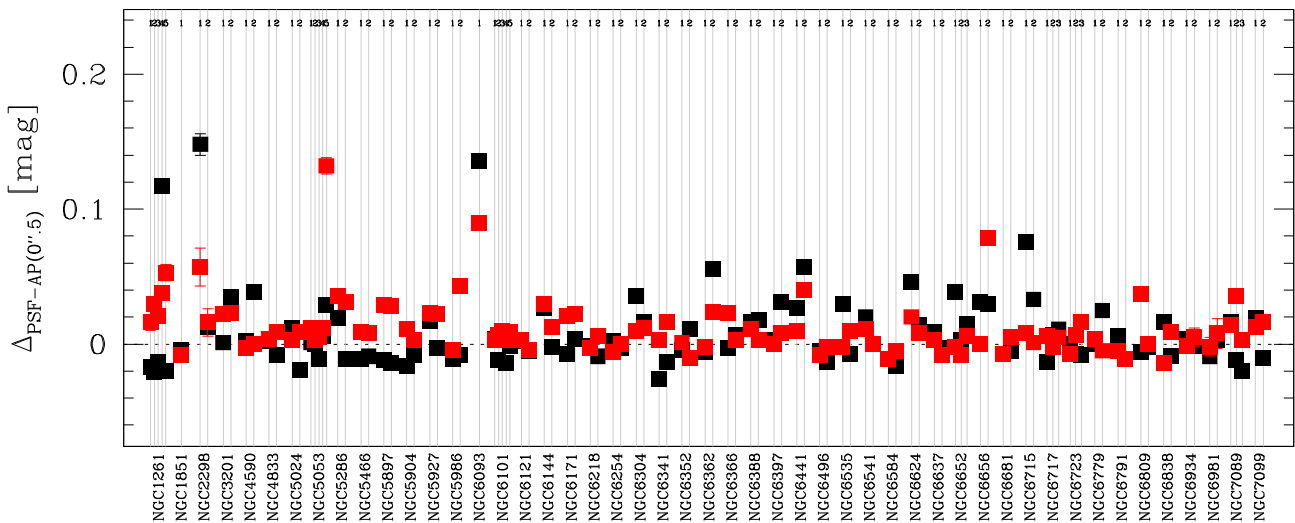


Figure 2. Aperture corrections measured in each field for each cluster. Red squares refer to $F475W$ observations, while black squares refer to $F814W$ ones.

*F*475*W* and one *F*814*W* image were taken each orbit, with a dither between the two dictated by primary WFC3 observing strategy. For each field, right ascension and declination of the centre of ACS/WFC are provided along with exposure time in each filter.

The physical position of ACS/WFC detectors in the focal plane of *HST* is such that its projected field of view (FoV) in the sky is located at a distance of about 6.5 arcmin from the centre of the WFC3 FoV. Depending on the number of orbits allocated to each GC, from two to a maximum of five non-overlapping fields were observed. This is because, in order to secure a good handling of charge-transfer-efficiency (CTE) systematic errors, primary WFC3 observations were taken by applying a different telescope rotation at each orbit ([Paper I](#), Section 4). For the majority of clusters, which were allocated two orbits, a rotation of about 90° was performed between the first and second orbit; for clusters observed for more than two orbits, a minimum difference of $\sim 45^\circ$ between the V3 PA of each orbit was required. Five distinct pointings were obtained for three clusters, namely NGC 1261, NGC 5053, and NGC 6101. Three distinct fields were obtained for four clusters: NGC 6652, NGC 6717, NGC 6723, and NGC 7089. For the other clusters, only two pointings were planned. M80 is an exception and was not observed as part of the Program GO-13297. For it, we make use of archival *HST* data from GO-12311. When possible, ACS parallel observations targeted pre-existing *HST* observations.

Figs 1 and A1–A8 display all *HST* observations that sample the sky area in the vicinity of those covered in this survey. Three cameras onboard *HST* were considered in order to enhance the probability of an overlap between observations: Wide Field and Planetary Camera 2 (WFPC2), ACS, and WFC3 (both UVIS and IR channels). Taking two images per orbit, one in $F475W$ and one in $F814W$ filters, the typical exposure times for both filters are of the order of 700 s.

All exposures have been corrected for CTE effects using the method described in Anderson & Bedin (2010). Photometric measurements of stellar objects in each field have been performed using a suite of FORTRAN programs based on `img2xym` (Anderson & King 2006) and `kitchen_sync` presented in Anderson et al. (2008). The spatial variation of the point spread function (PSF) has been taken into account adopting a grid of 9×10 model PSFs distributed along each image. However focus changes/breathing of the telescope, imperfect guiding, residual noise related to CTE can produce image-to-image variations of the PSF. To mitigate these sources of

systematic errors, we derived a set of spatially varying perturbations of the PSF models for each calibrated, non-drizzled ($f1c$) image. Adopting the procedure presented in Bellini et al. (2013), each image is divided into a grid with a number of cells changing from 2×2 to 5×5 . In each cell, a subset of well-measured stars is used to locally adjust the PSF models to the stellar profiles. Using an updated version of Anderson & King (2006) software, in combination with the newly created PSF models, we extracted raw catalogues of stellar positions and magnitudes in each image. We choose the grid refinement (between 2×2 to 5×5) that produces the best results, inspecting the distribution of the quality of fit parameters as a function of magnitude, and taking into account the number of reference stars used to tailor the PSF perturbations in each cell.

Each exposure related to the same field has been subsequently referred to a common reference frame. Since we are mainly interested in the faint, red part of the cluster CMDs, we used the *F814W* images to construct the reference frames. Catalogues are finally produced using a version of the software presented in Anderson et al. (2008), specifically tuned for this project. In particular, the `kitchen_sync` routine has been modified in order to work properly with only one image per filter. In addition, the method presented in Gilliland (2004) was applied in order to provide reliable photometry also for saturated stars.

The raw, instrumental magnitudes have been zero-pointed into ACS/WFC Vega-mag photometric system following the prescriptions of Bedin et al. (2005). The zero-points and aperture corrections from 0.5 arcsec to infinity of Bohlin (2016) have been used.

Especially in the present case, the photometric calibration plays a critical role, and we put strong efforts to precisely evaluate zero-point differences between various observations. Crowding is not a serious problem in the outer cluster regions and high-precision photometric measurements are relatively easy to obtain. But field-to-field zero-point variations must be accounted for to have the external fields of the same cluster on the same photometric scale. The main source of this photometric offsets between catalogues of distinct fields, is related to PSF modelling. The PSF model by construction is normalized to a surface flux of unity within a radius of 10 ACS/WFC pixels (0.5 arcsec). Only the inner 5×5 pixel region of sources was used to fit to the PSF model in order to minimize the contaminating impact of nearby neighbours, but any mismatch between the adopted PSF model and the pixels

Table 3. Precision reached with the re-derived astrometric solution using *Gaia* catalogues; for completeness we report the number of reference stars used. We also provide measures of the accuracy of the original STScI astrometric solution in the form of differences between RA and Dec.

#	Cluster	F	Stars	Precision (mas)	ΔRA WFC px	ΔDec. WFC px
01	NGC 1261	1	32	15.5	1.66 ± 0.34	-4.50 ± 0.16
		2	41	10.0	-1.89 ± 0.08	4.31 ± 0.21
		3	37	8.0	-0.51 ± 0.06	1.61 ± 0.18
		4	36	11.0	-0.50 ± 0.14	1.03 ± 0.31
		5	46	10.0	0.07 ± 0.05	-4.81 ± 0.19
02	NGC 1851	1 + 2	232	10.0	3.54 ± 0.20	-4.25 ± 0.19
03	NGC 2298	1	79	16.5	-0.17 ± 0.04	5.62 ± 0.24
		2	53	14.0	-0.11 ± 0.06	-1.37 ± 0.25
04	NGC 3201	1	635	13.0	0.14 ± 0.32	-0.57 ± 0.23
		2	653	10.0	4.33 ± 0.33	8.39 ± 0.20
05	NGC 4590	1	110	11.0	-0.78 ± 0.10	4.90 ± 0.15
		2	111	11.5	-0.12 ± 0.04	-3.86 ± 0.17
06	NGC 4833	1	492	7.0	-3.53 ± 0.35	6.86 ± 0.22
		2	570	6.5	1.75 ± 0.15	-0.02 ± 0.20
07	NGC 5024	1	173	11.5	-0.14 ± 0.23	3.09 ± 0.20
		2	142	10.0	-45.45 ± 0.77	1.35 ± 0.18
08	NGC 5053	1	44	9.5	0.72 ± 0.16	-0.62 ± 0.16
		2	41	8.0	-0.07 ± 0.15	-1.86 ± 0.18
		3	38	8.5	0.22 ± 0.13	0.29 ± 0.23
		4	42	10.0	0.43 ± 0.09	0.23 ± 0.19
		5	52	12.0	0.57 ± 0.16	-0.65 ± 0.16
09	NGC 5286	1	215	17.0	1.63 ± 0.20	1.85 ± 0.25
		2	217	16.5	1.61 ± 0.20	1.10 ± 0.21
10	NGC 5466	1	56	7.5	-0.13 ± 0.27	1.37 ± 0.12
		2	72	8.0	-0.79 ± 0.29	-2.22 ± 0.20
11	NGC 5897	1	164	9.0	0.12 ± 0.22	-0.37 ± 0.20
		2	154	7.5	2.58 ± 0.17	-2.51 ± 0.18
12	NGC 5904	1	579	7.0	-1.29 ± 0.19	-2.69 ± 0.15
		2	630	7.0	-0.16 ± 0.15	-1.08 ± 0.22
13	NGC 5927	1	848	8.5	3.65 ± 0.30	-0.38 ± 0.20
		2	985	8.0	-9.20 ± 0.35	11.91 ± 0.21
14	NGC 5986	1	278	8.0	-0.54 ± 0.30	1.36 ± 0.22
		2	268	6.0	-6.46 ± 0.26	4.12 ± 0.18
15	NGC 6093	1	236	22.0	1.81 ± 0.19	-4.47 ± 0.20
16	NGC 6101	1	235	7.0	-1.85 ± 0.76	1.09 ± 0.21
		2	232	6.5	-0.80 ± 0.61	2.90 ± 0.20
		3	229	8.0	-15.82 ± 0.73	0.55 ± 0.25
		4	263	11.0	-1.83 ± 0.89	-0.52 ± 0.27
		5	204	8.5	12.13 ± 0.85	-3.52 ± 0.24
17	NGC 6121	1	633	7.5	-4.81 ± 0.37	7.07 ± 0.23
		2	649	7.5	-0.69 ± 0.14	1.90 ± 0.22
18	NGC 6144	1	147	7.0	-4.48 ± 0.18	-0.10 ± 0.19
		2	147	9.5	-3.09 ± 0.15	-0.76 ± 0.20
19	NGC 6171	1	172	9.0	4.44 ± 0.20	-2.36 ± 0.16
		2	196	7.5	-3.26 ± 0.19	-1.51 ± 0.21
20	NGC 6218	1	300	10.0	0.40 ± 0.07	-4.05 ± 0.17
		2	362	6.5	-0.72 ± 0.09	0.13 ± 0.19
21	NGC 6254	1	525	7.5	-0.94 ± 0.11	2.02 ± 0.20
		2	507	5.0	-0.08 ± 0.12	-0.52 ± 0.18
22	NGC 6304	1	1021	11.0	0.00 ± 0.09	7.29 ± 0.22
		2	1137	11.0	-2.63 ± 0.15	3.66 ± 0.28
23	NGC 6341	1	272	7.0	3.31 ± 0.13	-1.46 ± 0.17
		2	276	6.5	1.30 ± 0.16	2.01 ± 0.14
24	NGC 6352	1	676	8.0	0.44 ± 0.09	6.24 ± 0.18
		2	658	9.5	0.20 ± 0.11	0.84 ± 0.21
25	NGC 6362	1	399	6.0	-1.98 ± 0.18	-1.19 ± 0.20
		2	412	6.0	-0.15 ± 0.23	2.51 ± 0.17
26	NGC 6366	1	265	7.0	1.07 ± 0.11	-4.03 ± 0.22
		2	263	6.0	2.89 ± 0.19	4.66 ± 0.18
27	NGC 6388	1	812	6.5	1.68 ± 0.24	4.01 ± 0.26

Table 3 – continued

#	Cluster	F	Stars	Precision (mas)	ΔRA WFC px	ΔDec. WFC px
28	NGC 6397	2	873	7.0	-0.86 ± 0.22	5.67 ± 0.22
		1	605	8.0	16.46 ± 0.47	12.42 ± 0.26
		2	602	7.0	-4.15 ± 0.33	4.79 ± 0.30
29	NGC 6441	1	1075	10.0	34.98 ± 0.54	-3.77 ± 0.26
30	NGC 6496	2	1114	9.5	4.46 ± 0.31	3.80 ± 0.27
		1	482	6.0	1.85 ± 0.30	7.03 ± 0.21
31	NGC 6535	2	525	9.0	8.00 ± 0.28	1.65 ± 0.22
		1	304	6.5	-4.97 ± 0.19	0.75 ± 0.18
32	NGC 6541	1	385	7.5	-11.12 ± 0.28	7.28 ± 0.23
		2	481	9.0	-7.23 ± 0.32	7.72 ± 0.22
33	NGC 6584	1	119	7.5	1.82 ± 0.19	6.15 ± 0.24
		2	141	10.0	2.67 ± 0.14	2.71 ± 0.25
34	NGC 6624	1	360	8.5	0.83 ± 0.12	1.93 ± 0.23
		2	774	9.5	0.61 ± 0.15	6.08 ± 0.21
35	NGC 6637	1	620	10.0	-3.66 ± 0.20	1.83 ± 0.25
		2	615	11.5	-2.54 ± 0.23	-0.80 ± 0.29
36	NGC 6652	1	608	12.0	0.35 ± 0.09	5.17 ± 0.26
		2	624	9.5	-0.06 ± 0.06	2.40 ± 0.25
37	NGC 6656	1	734	31.0	-1.20 ± 0.21	3.03 ± 0.25
		2	1052	27.5	1.21 ± 0.30	6.93 ± 0.31
38	NGC 6681	1	450	14.0	-4.20 ± 0.25	1.76 ± 0.29
		2	385	15.5	-2.37 ± 0.20	1.75 ± 0.32
39	NGC 6715	1	484	16.0	-0.69 ± 0.25	-4.67 ± 0.28
		2	505	15.5	3.28 ± 0.18	-1.79 ± 0.27
40	NGC 6717	1	439	14.0	3.48 ± 0.21	0.07 ± 0.30
		2	406	13.0	0.49 ± 0.20	1.11 ± 0.28
41	NGC 6723	1	256	14.5	0.14 ± 0.20	0.95 ± 0.30
		2	144	11.5	-0.25 ± 0.19	4.59 ± 0.22
42	NGC 6779	1	345	7.5	0.86 ± 0.07	1.07 ± 0.21
		2	333	6.5	3.24 ± 0.16	-8.92 ± 0.19
43	NGC 6791	1	288	9.0	-1.92 ± 0.26	-7.50 ± 0.21
		2	274	5.5	-4.98 ± 0.25	-6.18 ± 0.21
44	NGC 6809	1	584	7.0	-1.58 ± 0.19	0.99 ± 0.22
		2	590	7.5	-9.19 ± 0.21	-0.68 ± 0.23
45	NGC 6838	1	816	7.0	-8.81 ± 0.24	-12.24 ± 0.22
		2	800	6.5	-3.96 ± 0.22	-8.28 ± 0.21
46	NGC 6934	1	87	11.5	3.41 ± 0.20	2.62 ± 0.24
		2	84	5.5	1.41 ± 0.10	-12.00 ± 0.17
47	NGC 6981	1	31	14.5	1.29 ± 0.26	-9.37 ± 0.19
		2	27	9.5	1.73 ± 0.23	-8.07 ± 0.23
48	NGC 7089	1	92	5.5	-0.55 ± 0.12	-6.84 ± 0.15
		2	77	10.5	2.52 ± 0.15	-1.40 ± 0.18
		3	82	11.0	1.85 ± 0.12	-0.54 ± 0.20
49	NGC 7099	1	79	4.5	0.93 ± 0.08	-0.89 ± 0.17
		2	89	6.5	0.66 ± 0.08	1.75 ± 0.21

beyond the small square fitting aperture would result in a slight zero-point shift. The fact that we perturb the library PSFs (above) minimizes this even further. However, the best way to regularize the photometry is empirically: following Bedin et al. (2005) and Anderson et al. (2008), we measured aperture corrections inside this aperture using the calibrated and drizzled (`drc`) images as reference.

These corrections were sufficient to properly take into account the majority of the photometric biases in our catalogues. The obtained values of the aperture correction for an aperture of 0.5 arcsec are listed in Table 2. We maintain the same nomenclature as in

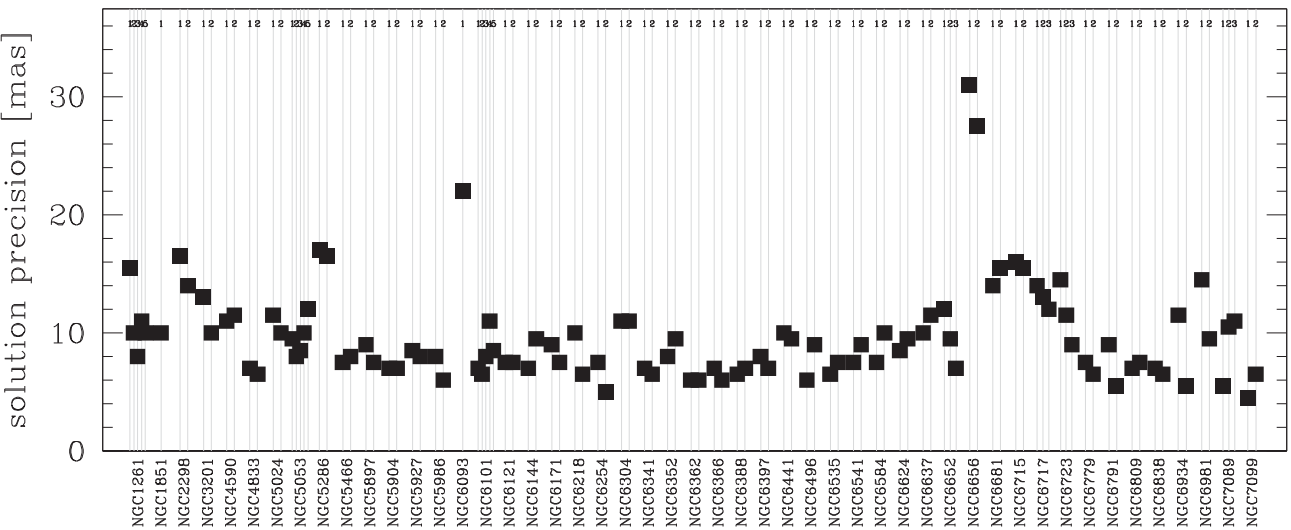


Figure 3. Precision of the redefined astrometric solution for each observed field, see the text for details.

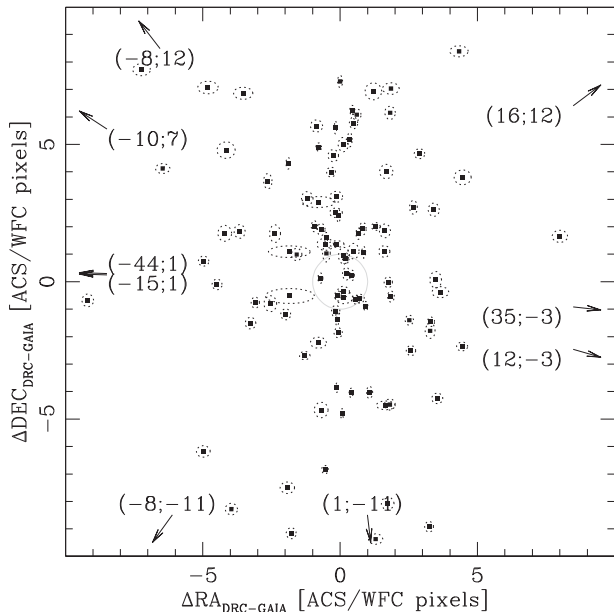


Figure 4. Offsets between star positions obtained using the original STScI astrometric solution (header of `drz` images) and *Gaia* ones. Points represent single fields; the semi-axes of each ellipse have length equal to the measured standard deviation. The grey circle represents an offset of 1 ACS/WFC pixel, which corresponds to ~ 0.05 arcsec. Some points fall outside the used limits; we indicate their position along the edges of the figure, the arrows point in their direction.

Bedin et al. (2005). The aperture correction values, along with their associated uncertainties are also reported in Fig. 2. Black dots are referred to $F814W$ observations, red dots to $F475W$ ones. It can be noted that for the majority of cases corrections are small: typically smaller than 0.04 magnitudes, but in the most severe cases, they can reach values as high as 0.15 mag.

Astrometrized, stacked images of each observed field have also been produced for both filters with a 1×1 pixel sampling. These have been created, for each field, combining all overlapping f1c images using the same coordinate transformations that define the common reference frames.

Astrometric solutions have been independently derived using the *Gaia* DR1 catalogue as a reference (Gaia Collaboration 2016). As a consequence, positions are given for Equinox J2000 at epoch 2015. Table 3 reports the precision reached by the new astrometric solution in the fifth column, which is the root mean square error of the offset between *Gaia* positions and those derived, for the same stars, in our astrometrized stacked images. The measured average value is 0.2 pixel, or ~ 10 milliarcsec. These values are also visualized in Fig. 3.

For completeness, we also measure the astrometric precision of the original astrometric solution of `drc` images. The position offset between common sources in the *Gaia* DR1 catalogue and the `drc` images is used to define this quantity. Offset values are referred to RA and Dec. distances in image pixels and are reported in columns six and seven of Table 3. The associated errors corresponds to the measured standard deviations of each sample. A visual representation is also given in Fig. 4. It can be noted that, in general, offsets are lower than 5 ACS/WFC pixels (0.25 arcsec), and, in many cases, below 1 pixel, with some notable exceptions.

3 THE COLOUR-MAGNITUDE DIAGRAMS AND TRICHROMATIC STACKED IMAGES

In Fig. 5 we report the CMDs obtained for all five fields of NGC 1261. Magnitudes are given both in the instrumental and Vega-mag photometric systems. Dashed lines represent the saturation limit, black dots represent unsaturated stars, saturated stars are represented with crosses. The five CMDs are all merged in the bottom-right panel, where a different colour have been assigned to each different field. In this case, the instrumental magnitude scale, along with saturation level (dashed line), refer only to Field 1.

The final CMDs for all other targets are presented in Figs A9–A16. The presented CMDs have been obtained by selecting only high-quality stars, according to quality parameters presented in Anderson et al. (2008). In Section 4 we describe the adopted selection procedure. It is important to mention here that, since in the majority of the cases only one image per filter has been taken, artefact rejection is not an easy task. In order to include faint sources, we have chosen not to limit in flux our raw catalogues. We none the less restricted the detections only to those sources observed in at least

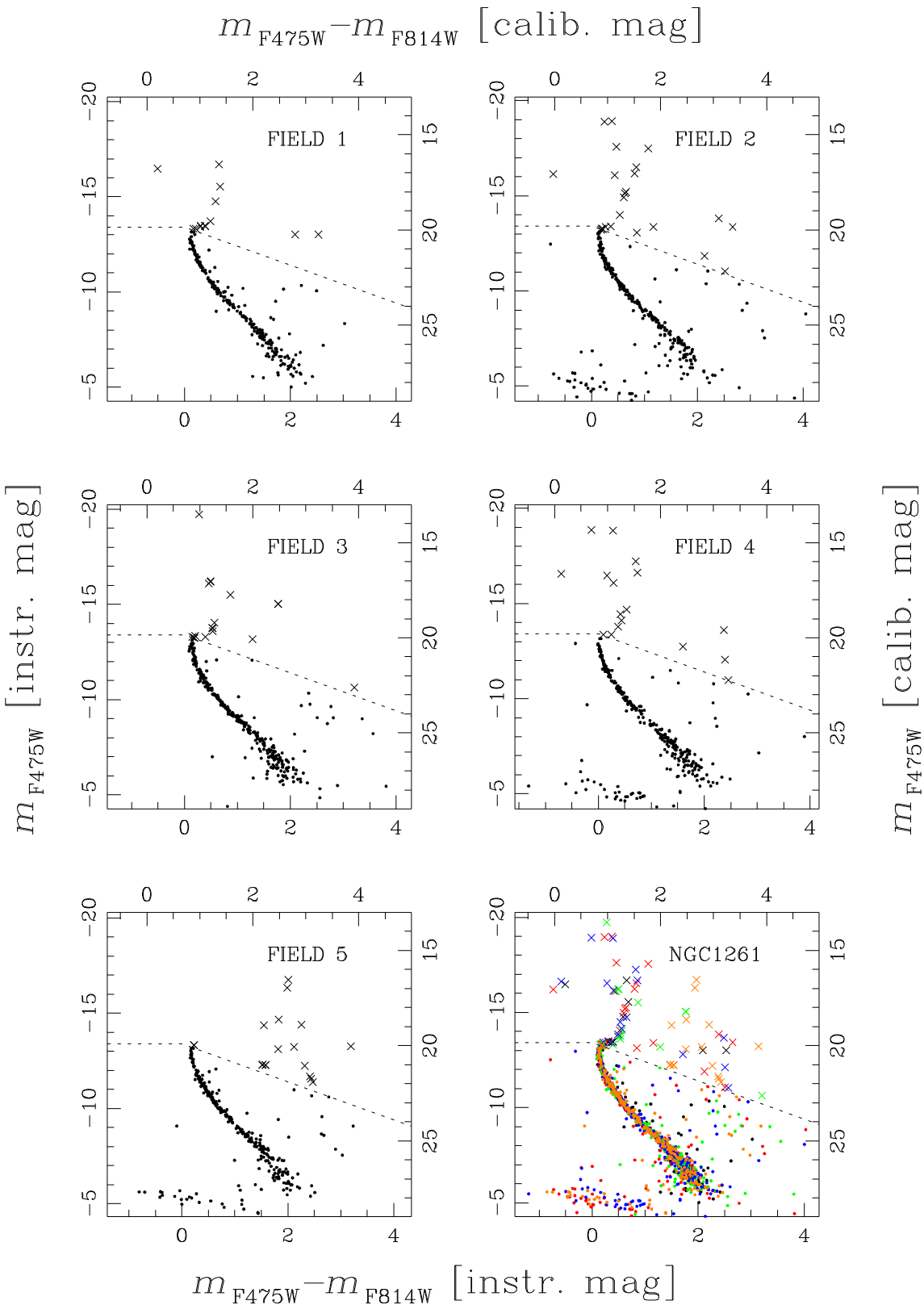


Figure 5. CMDs of the parallel fields of NGC 1261. Both instrumental and calibrated magnitude scales are shown. Dashed lines represent the saturation levels. Saturated stars are marked with crosses. The bottom-right panel collects all the stars present in all the five fields. Stars are here colour-coded as follows. Black dots represent stars measured in F1, red dots stars of F2, green dots stars of F3, blue dots stars of F4, and orange dots represent stars measured in F5. The instrumental magnitude scale and the saturation limit refer to F1 only.

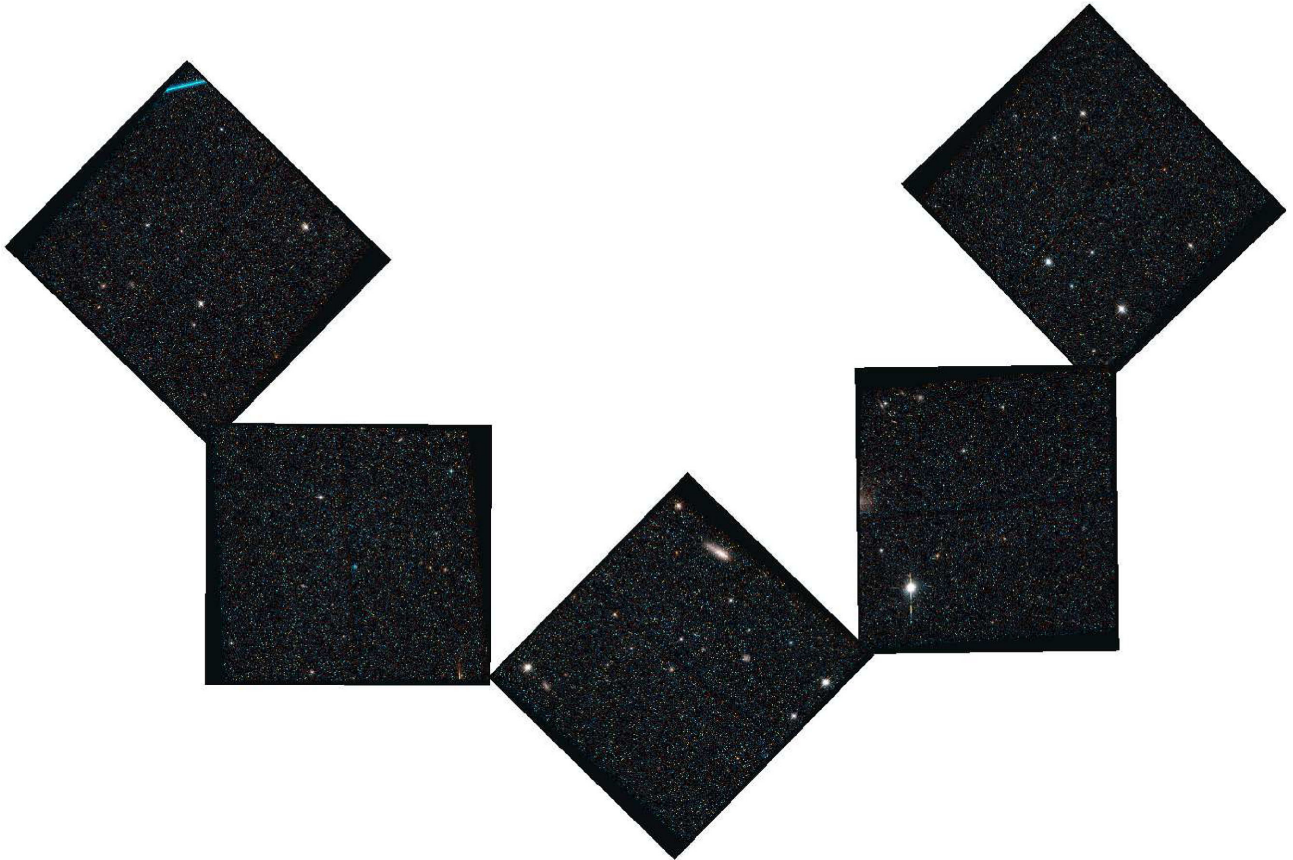


Figure 6. Mosaic of all trichromatic images created for NGC 1261; see the text for details.

one $F814W$ and one $F475W$ image simultaneously, with positions in the common reference frame consistent within 0.8 pixels.

No rejection of foreground/background contamination has been performed, nor any correction for differential reddening. The homogeneity of the data guarantees very similar results in every case. None the less, it is out of the scope of this work to characterize in detail the obtained results, which require taking into consideration several issues. For example, the number density of cluster members present in the observed fields depends on the properties of each GC: in some cases, especially for bulge clusters, or those that appear projected in this dense Galactic region, it is difficult to identify the cluster sequence. We recall that another interesting application of the present data is the study of the stellar populations, external to the clusters, that contaminate the observed fields. In particular, for at least six GCs, namely NGC 6624, NGC 6637, NGC 6652, NGC 6681, NGC 6715, and NGC 6809, traces of the Sagittarius Stream are visible in the obtained CMDs (Siegel et al. 2011).

As an additional tool to explore and characterize observations, we have created colour images of each observed field, combining the astrometrized stacked images: an example is shown in Fig. 6. The $F814W$ stacked images have been associated with red channel while the $F475W$ images are associated with the blue channel. The images associated with the green channel have been obtained as a result of a 3:1 weighted mean of $F475W$ and $F814W$ counts, respectively.

4 SELECTION OF WELL-MEASURED STARS

This section describes the procedure adopted to reject spurious or poorly measured sources in the catalogues and to obtain a sample of

bona-fide stellar sources. In this example we refer to the catalogue associated with Field 1 of NGC 6121 (M4). The V3 PA is 272 deg and, for this field, two images were collected, one in $F814W$, and the other in $F475W$ (666 and 739 s, respectively).

For the selection, we have adopted a procedure similar to that described in Milone et al. (2012), defining limits in both q and o (quality) parameters. In addition, we also made use of the *RADXS* parameter (Bedin et al. 2008, 2009, 2010).

As shown in the lower left panels of Fig. 7, the q parameter displays a characteristic trend with magnitude. This parameter is defined as the absolute value of the subtraction between the PSF model and the spatial distribution of light of a particular detection in the image, inside the fitting radius. For a perfectly modelled source, the q parameter assumes value 0.

The o parameter quantifies the amount of light that falls on the aperture used for PSF fitting, due to neighbouring sources (Anderson et al. 2008). Unlike the q parameter, it does not show a clear trend with magnitude (middle-left panels of Fig. 7), for this reason we have used a fixed limit (Milone et al. 2012).

Finally, the *RADXS* parameter is related to the spatial extent of the sources, and it is used to distinguish between point sources and extended sources. It is defined as the flux in excess of that predicted from the PSF fitting just outside the core of each source (Bedin et al. 2008). Positive values are expected for extended objects, while negative values indicate detections that are sharper than stellar. The introduction of this parameter in the selection process for the present case is particularly necessary: since only one image per filter is available for most cases, spurious detections due to cosmic rays are present in the catalogues. Moreover, these observations cover the external regions of GCs, where the stellar density is not as high as in

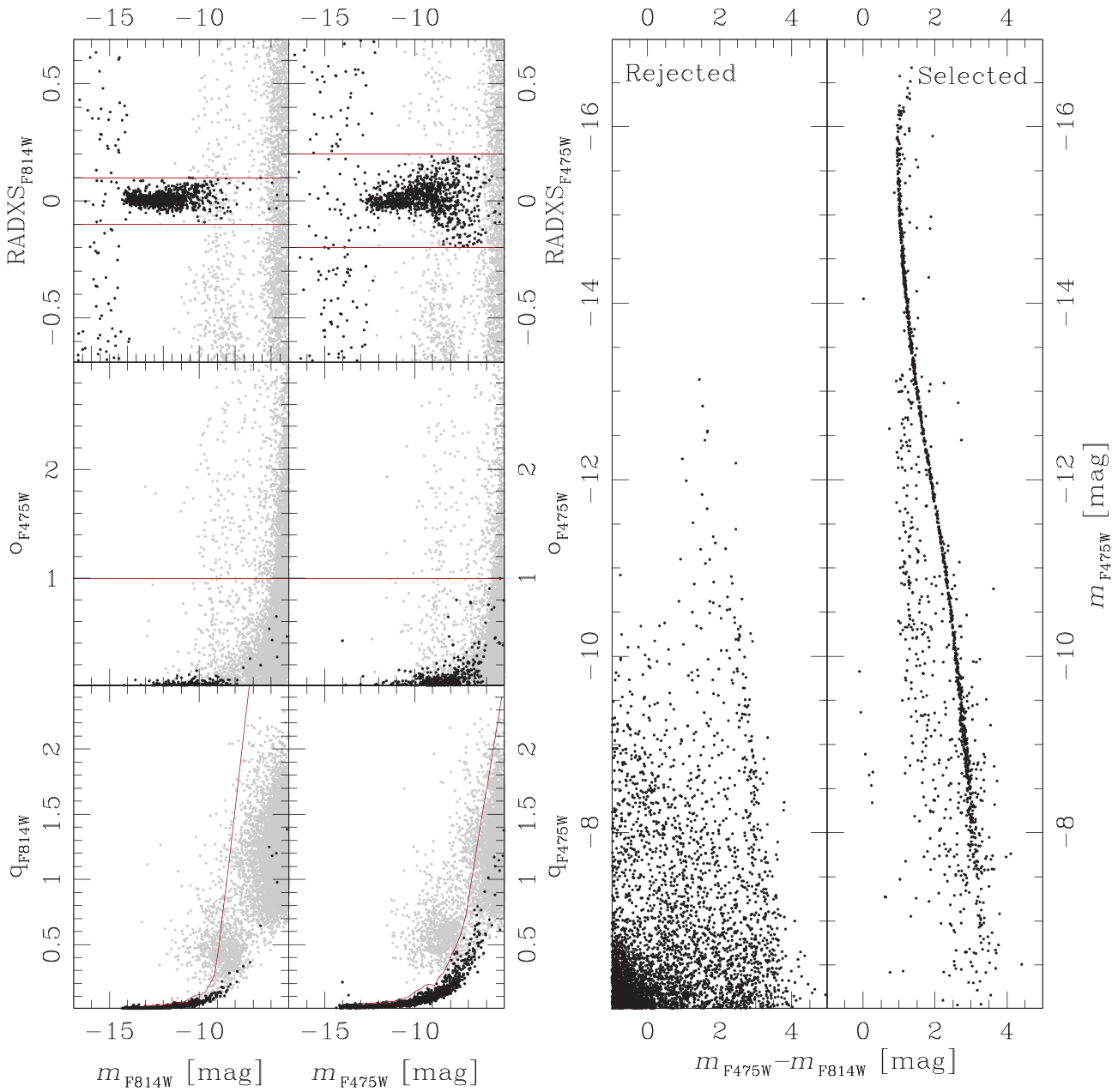


Figure 7. Selection procedure for Field 1 of NGC 6121. Left-hand panels: black points mark the stars that were selected as well-measured. Red lines mark the limits chosen for the q , o , and $RADXS$ parameters. Second panel from right: CMD of rejected sources. Right-hand panel: CMD with only sources that survived the selection. All plots refer to instrumental magnitudes.

the central regions. The observed fields are thus relatively populated by extragalactic, non-stellar objects.

We started by taking a more stringent limit in position-consistency for each source. We selected only sources with an rms error in position less than 0.3 pixel. We adopted fixed limits in the o and $RADXS$ parameters for both filters simultaneously. Finally, we measured, for the sources that survived this first selection, the median trend in the plane defined by magnitude and q parameter values. In this way, we removed from the sample non-stellar and poorly measured sources, while not a priori losing faint sources. Red lines in the left-hand panels of Fig. 7 represent the limits used for the case of Field 1 of NGC 6121 (M4). Black points represent sources that passed the selection process. The CMD corresponding

to rejected sources (grey dots in the left-hand panels) is shown in the second panel from the right.

The resulting CMD is shown in the right-hand panel of Fig. 7. Note how the cleaning process allows the clear detection of the white-dwarf cooling sequence. Saturated stars have been excluded from the selection procedure, but their fluxes have been recovered using the procedure described in Gilliland (2004).

5 RELEASED ELECTRONIC MATERIAL

We release, for each ACS/WFC parallel field, the astrometric and photometric catalogues and trichromatic astrometrized stacked images. All the released material will be available for download at

the website of the Exoplanets & Stellar Populations Group of the Università degli Studi di Padova.¹

Table 4 shows the first 10 rows of the catalogue produced for Field 1 of NGC 6121. The content of each column is explained in detail in Table 5. The parameters *wi* and *wb* are the same as in Anderson et al. (2008). They are records that represent the level of saturation of each source in *F814W* and *F475W* images, respectively. The last column includes the results of the selection of well-measured stars presented in Section 4.

Note that for many stars, we report a magnitude rms error of 9.900. This is because the routine empirically determines errors based on multiple observations in each filter. When there is only one observation per filter, the error is given a high default value.

6 SUMMARY AND CONCLUSIONS

In the context of the *Hubble Space Telescope* UV Legacy Survey Treasury program of Galactic Globular Clusters (GO-13297; PI: Piotti, Paper I), we are releasing the photometric catalogues relative to the ACS/WFC parallel observations. They represent the first *HST* photometric survey of external regions of Galactic GCs and consist of 109 distinct stellar fields of 49 targets: 48 GCs and one open cluster, NGC 6791.

In the majority of cases, only two images per field were taken, one in *F814W* and other in *F475W*, centred at about 6.5 arcmin from cluster centre. Exposure times were selected in order to obtain reliable photometry of the main sequence of target GCs.

These observations complement the WFC3 observations of the central regions of the surveyed GCs, and represent valuable tools for different investigations as outlined in Paper I. These data represent a first epoch for future studies aimed at proper motions measurements in these regions. Even without proper motions, these catalogues are suitable to various interesting studies such as measurements of mass functions and binaries fractions in external regions of GCs. Furthermore, crowding is not an issue in these external cluster fields, as a result, this data base could be also used as an input list for spectroscopic follow-up, for example for precise chemical tagging of cluster members.

ACKNOWLEDGEMENTS

We thank the anonymous referee for his careful revision that improved the quality of the present manuscript. MS, AA, and GP acknowledge support from the Spanish Ministry of Economy and Competitiveness (MINECO) under grant AYA2013-42781. MS and AA acknowledge support from the Instituto de Astrofísica de Canarias (IAC) under grant 309403. GP acknowledges partial support by the Università degli Studi di Padova Progetto di Ateneo CPDA141214 ‘Towards understanding complex star formation in Galactic globular clusters’ and by INAF under the program PRIN-INAF2014. APM acknowledges support by the Australian Research Council through Discovery Early Career Researcher Award DE150101816 and by the ERC-StG 2016 716082 project ‘GALFOR’ funded by the European Research Council. This work has made use of data from the European Space Agency (ESA) mission *Gaia* (<http://www.cosmos.esa.int/gaia>), processed by the *Gaia* Data Processing and Analysis Consortium (DPAC, <http://www.cosmos.esa.int/web/gaia/dpac/consortium>). Funding for the DPAC has been provided by national institutions, in

#id	RA (2015)	Dec. (2015)	x	dx	y	dy	<i>F814W</i>	<i>id</i>	<i>db</i>	<i>qb</i>	<i>qi</i>	<i>db</i>	<i>qb</i>	<i>qi</i>	<i>RADSXi</i>	<i>RADSXb</i>	<i>mi</i>	<i>mb</i>	<i>wi</i>	<i>wb</i>	Good	
00000001	-26.47807749	-26.47823845	549416	0.353	6881174	0.224	28.832	9.900	0.152	0.088	0.088	0.152	0.088	27.109	9.900	0.336	0.336	0.423	0.423	0.322	26.991	9.900
00000002	-26.47896240	-26.47961100	687260	0.632	691807	0.224	27.164	9.900	0.152	0.076	0.076	0.152	0.076	28.421	9.900	0.337	0.337	0.426	0.426	0.354	26.711	9.900
00000003	-26.47896280	-26.47961130	687264	0.632	691807	0.224	27.164	9.900	0.152	0.076	0.076	0.152	0.076	28.421	9.900	0.337	0.337	0.426	0.426	0.354	26.730	9.900
00000004	-26.47896300	-26.47961150	687268	0.632	691807	0.224	27.164	9.900	0.152	0.076	0.076	0.152	0.076	28.421	9.900	0.337	0.337	0.426	0.426	0.354	26.730	9.900
00000005	-26.47896320	-26.47961170	687272	0.632	691807	0.224	27.164	9.900	0.152	0.076	0.076	0.152	0.076	28.421	9.900	0.337	0.337	0.426	0.426	0.354	26.730	9.900
00000006	-26.47896340	-26.47961190	687276	0.632	691807	0.224	27.164	9.900	0.152	0.076	0.076	0.152	0.076	28.421	9.900	0.337	0.337	0.426	0.426	0.354	26.730	9.900
00000007	-26.47896360	-26.47962210	687280	0.632	691807	0.224	27.164	9.900	0.152	0.076	0.076	0.152	0.076	28.421	9.900	0.337	0.337	0.426	0.426	0.354	26.730	9.900
00000008	-26.47896380	-26.47962230	687284	0.632	691807	0.224	27.164	9.900	0.152	0.076	0.076	0.152	0.076	28.421	9.900	0.337	0.337	0.426	0.426	0.354	26.730	9.900
00000009	-26.47896400	-26.47962250	687288	0.632	691807	0.224	27.164	9.900	0.152	0.076	0.076	0.152	0.076	28.421	9.900	0.337	0.337	0.426	0.426	0.354	26.730	9.900
00000010	-26.47896420	-26.47962270	687292	0.632	691807	0.224	27.164	9.900	0.152	0.076	0.076	0.152	0.076	28.421	9.900	0.337	0.337	0.426	0.426	0.354	26.730	9.900

Table 4. First 10 rows extracted from the catalogue referring to Field 1 of NGC 6121 (M4). A detailed description of each column is given in Table 5.

¹ <http://groups.dfa.unipd.it/ESPG/treasury.php>

Table 5. Information provided by each catalogue.

Col.	Name	Explanation
01	id	ID number for each star
02	RA	Right ascension for each star (in deg, epoch 2015)
03	Dec.	Declination for each star (in deg, epoch 2015)
04	x	x position of each star on the reference frame (in pixels)
05	dx	rms errors associated with x position (in pixels)
06	y	y position of each star on the reference frame (in pixels)
07	dy	rms errors associated with y position (in pixels)
08	F814W	F814W magnitude calibrated into Vegamag system
09	di	rms errors associated with F814W magnitude
10	F475W	F475W magnitude calibrated into Vegamag system
11	db	rms errors associated with F475W magnitude
12	qi	q parameter for F814W magnitudes
13	qb	q parameter for F475W magnitudes
14	oi	o parameter for F814W magnitudes
15	ob	o parameter for F475W magnitudes
16	RADXS _i	RADXS parameter for F814W
17	RADXS _b	RADXS parameter for F475W
18	ni	Number of F814W images the source has been detected in
19	nb	Number of F475W images the source has been detected in
20	wi	Source of F814W photometry 1: unsaturated in deep; 2: unsaturated in short; 3: saturated in short; 4: saturated in deep;
21	wb	Source of F475W photometry (same as wi)
22	good	The source has passed the selection process

particular the institutions participating in the *Gaia* Multilateral Agreement.

Based on observations with the NASA/ESA *Hubble Space Telescope*, obtained at the Space Telescope Science Institute, which is operated by AURA, Inc., under NASA contract NAS 5-26555.

REFERENCES

- Anderson A. J. 1997, PhD thesis, Univ. California, Berkeley
- Anderson J., Bedin L. R., 2010, *PASP*, 122, 1035
- Anderson J., King I. R., 2006, Instrument Science Report ACS 2006-01, 34
- Anderson J. et al., 2008, *AJ*, 135, 2055
- Bedin L. R., Piotto G., Anderson J., Cassisi S., King I. R., Momany Y., Carraro G., 2004, *ApJ*, 605, L125
- Bedin L. R., Cassisi S., Castelli F., Piotto G., Anderson J., Salaris M., Momany Y., Pietrinferni A., 2005, *MNRAS*, 357, 1038
- Bedin L. R., King I. R., Anderson J., Piotto G., Salaris M., Cassisi S., Serenelli A., 2008, *ApJ*, 678, 1279
- Bedin L. R., Salaris M., Piotto G., Anderson J., King I. R., Cassisi S., 2009, *ApJ*, 697, 965
- Bedin L. R., Salaris M., King I. R., Piotto G., Anderson J., Cassisi S., 2010, *ApJ*, 708, L32
- Bellini A., Piotto G., Bedin L. R., King I. R., Anderson J., Milone A. P., Momany Y., 2009, *A&A*, 507, 1393
- Bellini A., Bedin L. R., Piotto G., Milone A. P., Marino A. F., Villanova S., 2010, *AJ*, 140, 631
- Bellini A., Anderson J., Salaris M., Cassisi S., Bedin L. R., Piotto G., Bergeron P., 2013, *ApJ*, 769, L32
- Bohlin R. C., 2016, *AJ*, 152, 60
- Carretta E. et al., 2009a, *A&A*, 505, 117
- Carretta E., Bragaglia A., Gratton R., Lucatello S., 2009b, *A&A*, 505, 139
- Cassisi S., Salaris M., Pietrinferni A., Hyder D., 2017, *MNRAS*, 464, 2341
- D'Ercole A., Vesperini E., D'Antona F., McMillan S. L. W., Recchi S., 2008, *MNRAS*, 391, 825
- Gaia Collaboration, 2016, *A&A*, 595, A2
- Gilliland R. L., 2004, Instrument Science Report ACS 2004-01, 18
- Gratton R. G., Carretta E., Bragaglia A., 2012, *A&AR*, 20, 50
- Gratton R., Sneden C., Carretta E., 2004, *ARA&A*, 42, 385
- Harris W. E., 1996, *AJ*, 112, 1487
- Kraft R. P., 1994, *PASP*, 106, 553
- Lee Y.-W., Joo J.-M., Sohn Y.-J., Rey S.-C., Lee H.-C., Walker A. R., 1999, *Nature*, 402, 55
- Marino A. F., Villanova S., Piotto G., Milone A. P., Momany Y., Bedin L. R., Medling A. M., 2008, *A&A*, 490, 625
- Milone A. P. et al., 2008, *ApJ*, 673, 241
- Milone A. P. et al., 2012, *A&A*, 540, A16
- Milone A. P. et al., 2017, *MNRAS*, 464, 3636 (Paper IX)
- Pancino E., Ferraro F. R., Bellazzini M., Piotto G., Zoccali M., 2000, *ApJ*, 534, L83
- Paust N. E. Q. et al., 2010, *AJ*, 139, 476
- Piotto G. et al., 2002, *A&A*, 391, 945
- Piotto G. et al., 2007, *ApJ*, 661, L53
- Piotto G. et al., 2015, *AJ*, 149, 91 (Paper I)
- Rosenberg A., Piotto G., Saviane I., Aparicio A., 2000a, *A&AS*, 144, 5
- Rosenberg A., Aparicio A., Saviane I., Piotto G., 2000b, *A&AS*, 145, 451
- Sarajedini A. et al., 2007, *AJ*, 133, 1658
- Sbordone L., Salaris M., Weiss A., Cassisi S., 2011, *A&A*, 534, A9
- Siegel M. H. et al., 2011, *ApJ*, 743, 20
- Simioni M., Milone A. P., Bedin L. R., Aparicio A., Piotto G., Vesperini E., Hong J., 2016, *MNRAS*, 463, 449
- Sollima A., Baumgardt H., 2017, *MNRAS*, 471, 3668
- Vesperini E., Heggie D. C., 1997, *MNRAS*, 289, 898
- Vesperini E., McMillan S. L. W., D'Antona F., D'Ercole A., 2013, *MNRAS*, 429, 1913
- Yong D., Grundahl F., 2008, *ApJ*, 672, L29

APPENDIX A: EXTRA MATERIAL

In this section we complement Figs 1 and 5 with those referred to the rest of the sample. In particular, Figs A1–A8 complement the sample of finding charts presented in Fig. 1. Figs A9–A16 are analogues to the lower right panel of Fig. 5.

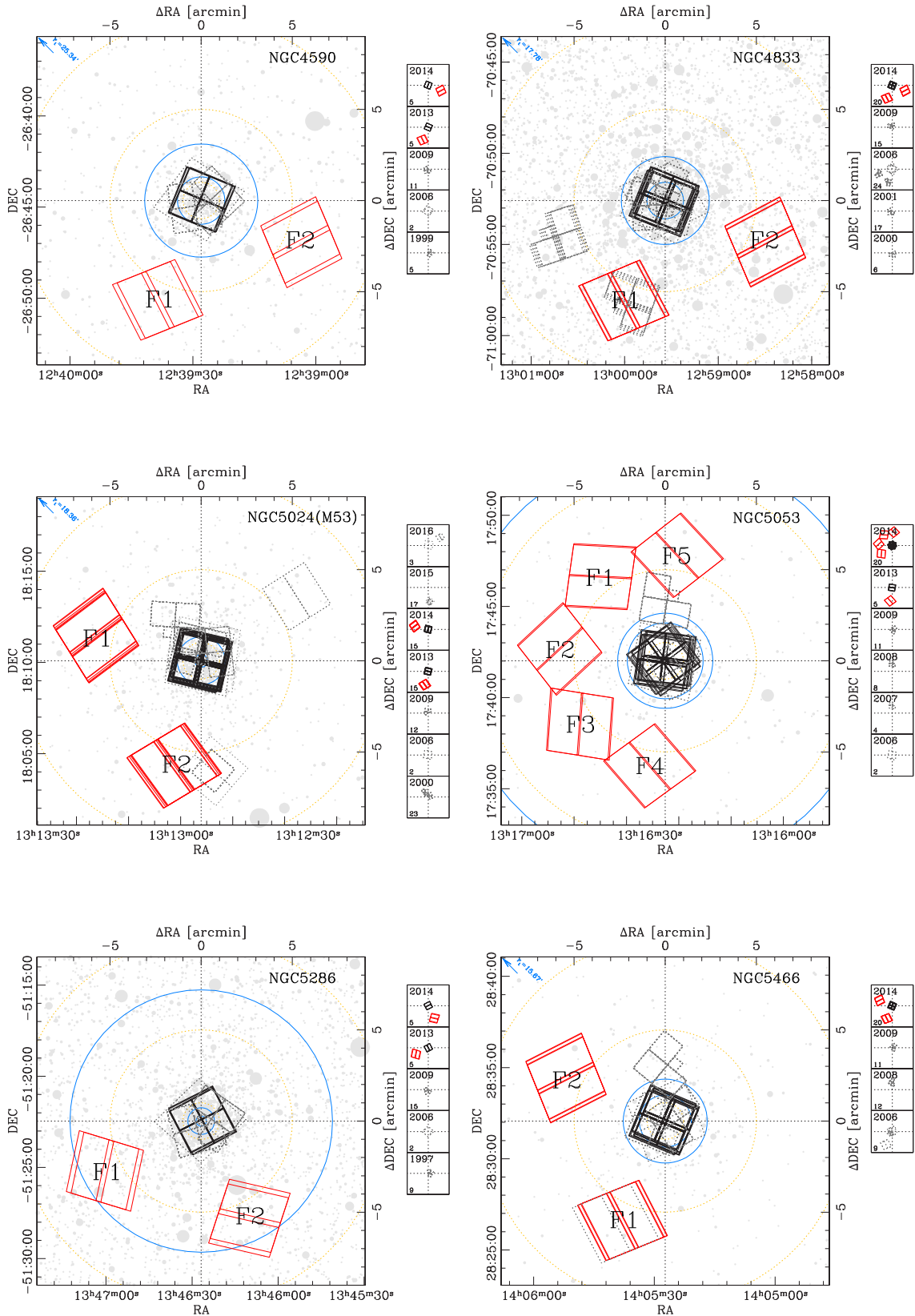


Figure A1. As in Fig. 1 but for NGC 4590, NGC 4833, NGC 5024, NGC 5053, NGC 5286, and NGC 5466.

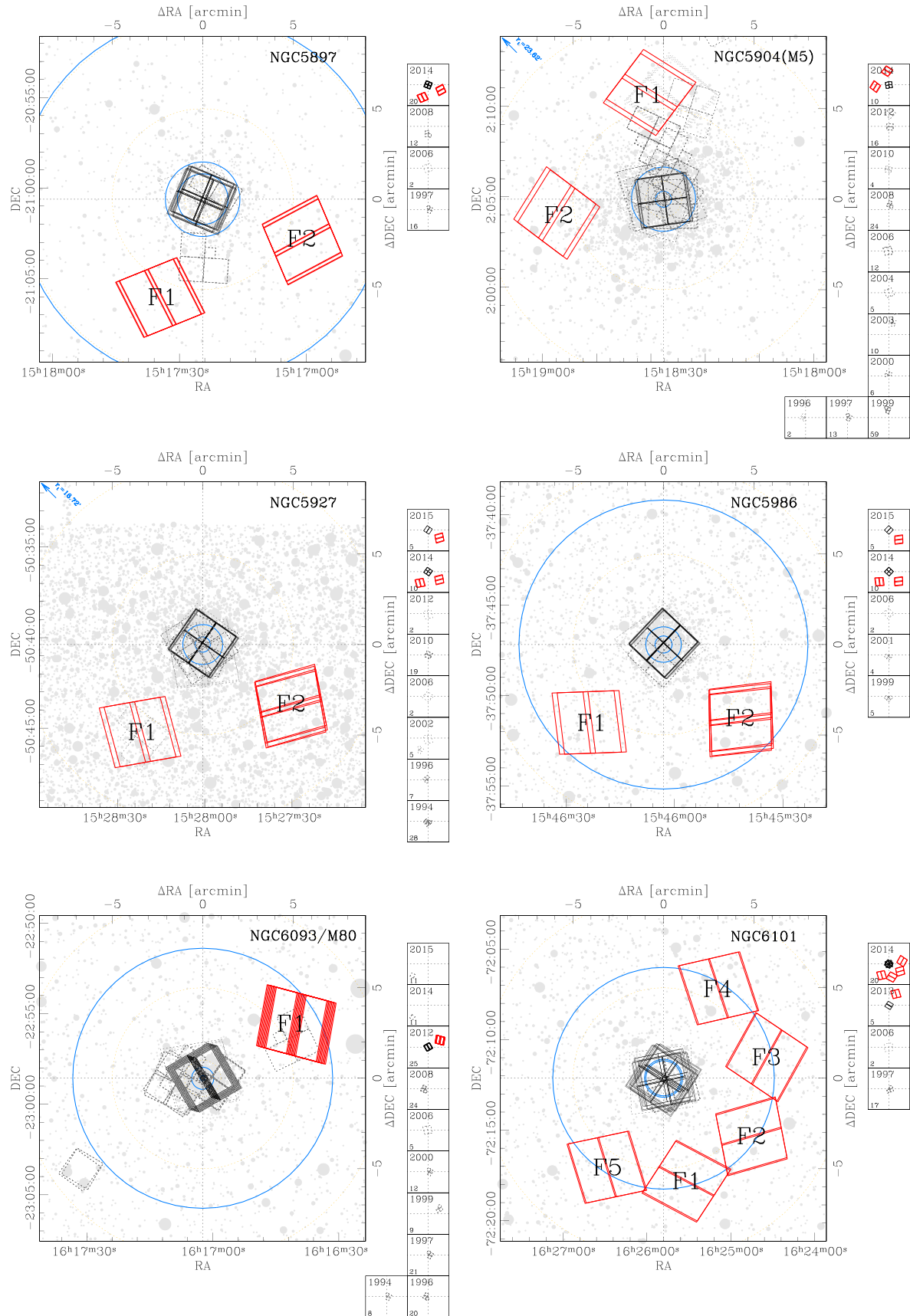


Figure A2. As in Fig. 1 but for NGC 5897, NGC 5904, NGC 5927, NGC 5986, NGC 6093, and NGC 6101.

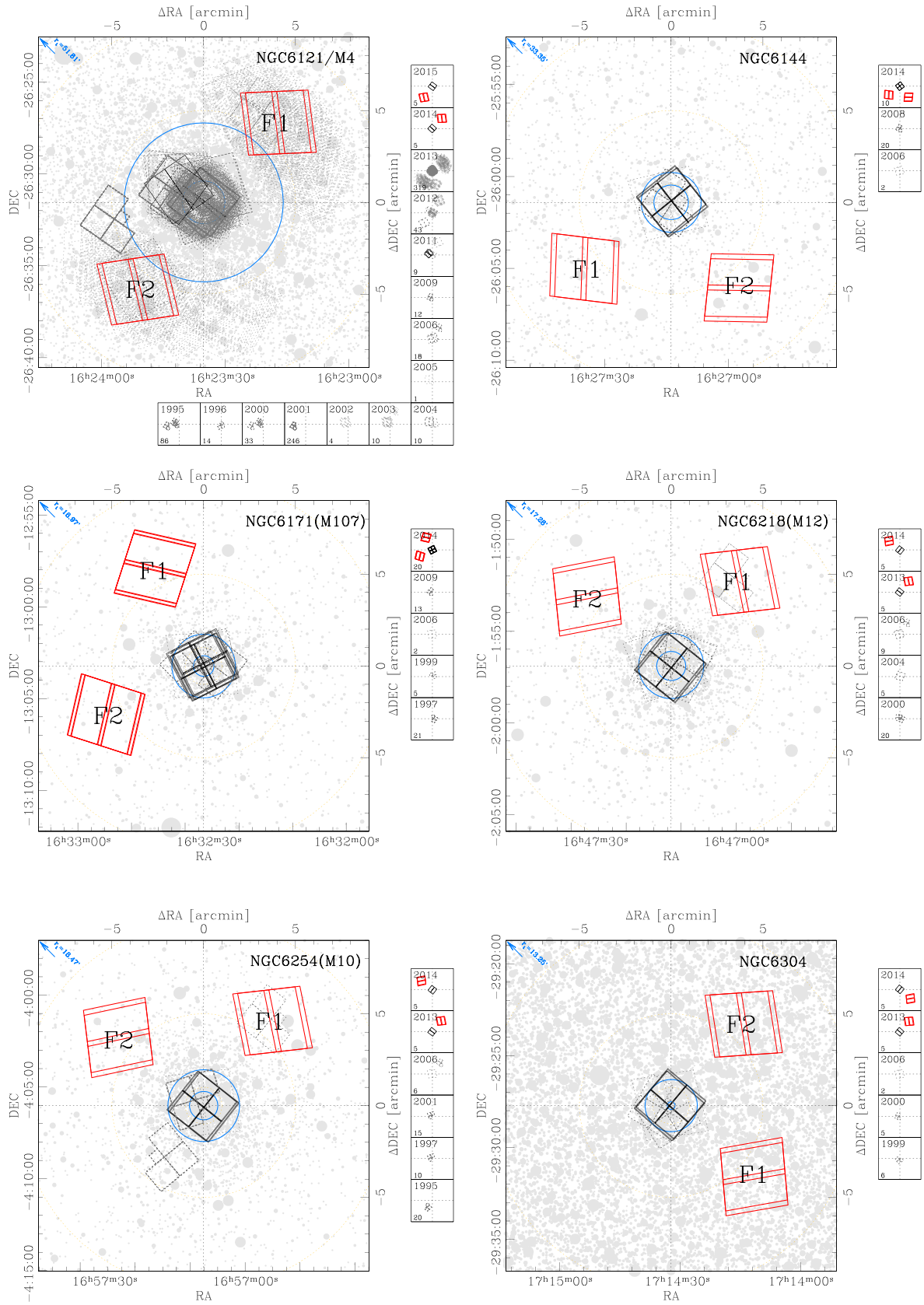


Figure A3. As in Fig. 1 but for NGC 6121, NGC 6144, NGC 6171, NGC 6218, NGC 6254, and NGC 6304.

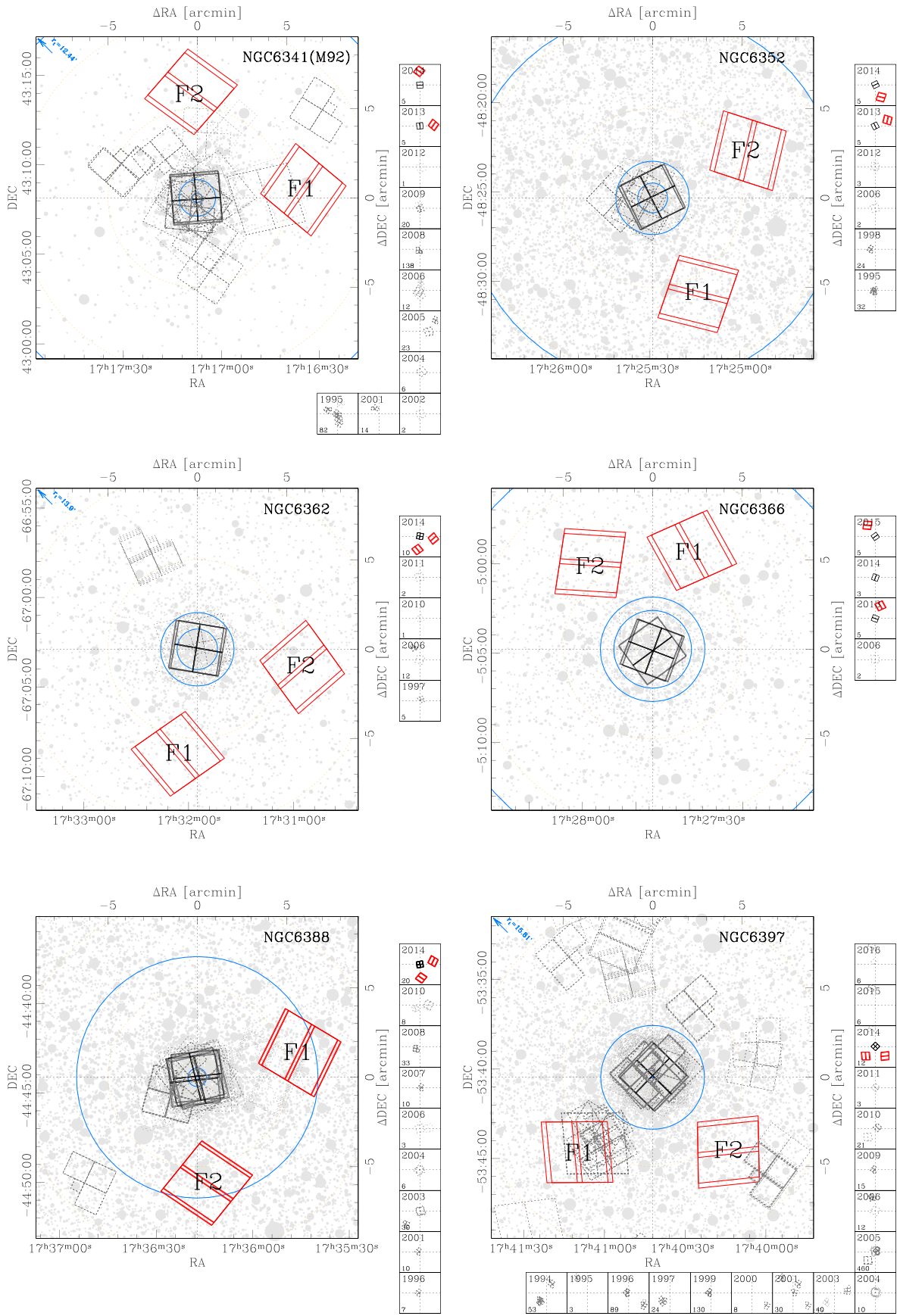


Figure A4. As in Fig. 1 but for NGC 6341, NGC 6352, NGC 6362, NGC 6366, NGC 6388, and NGC 6397.

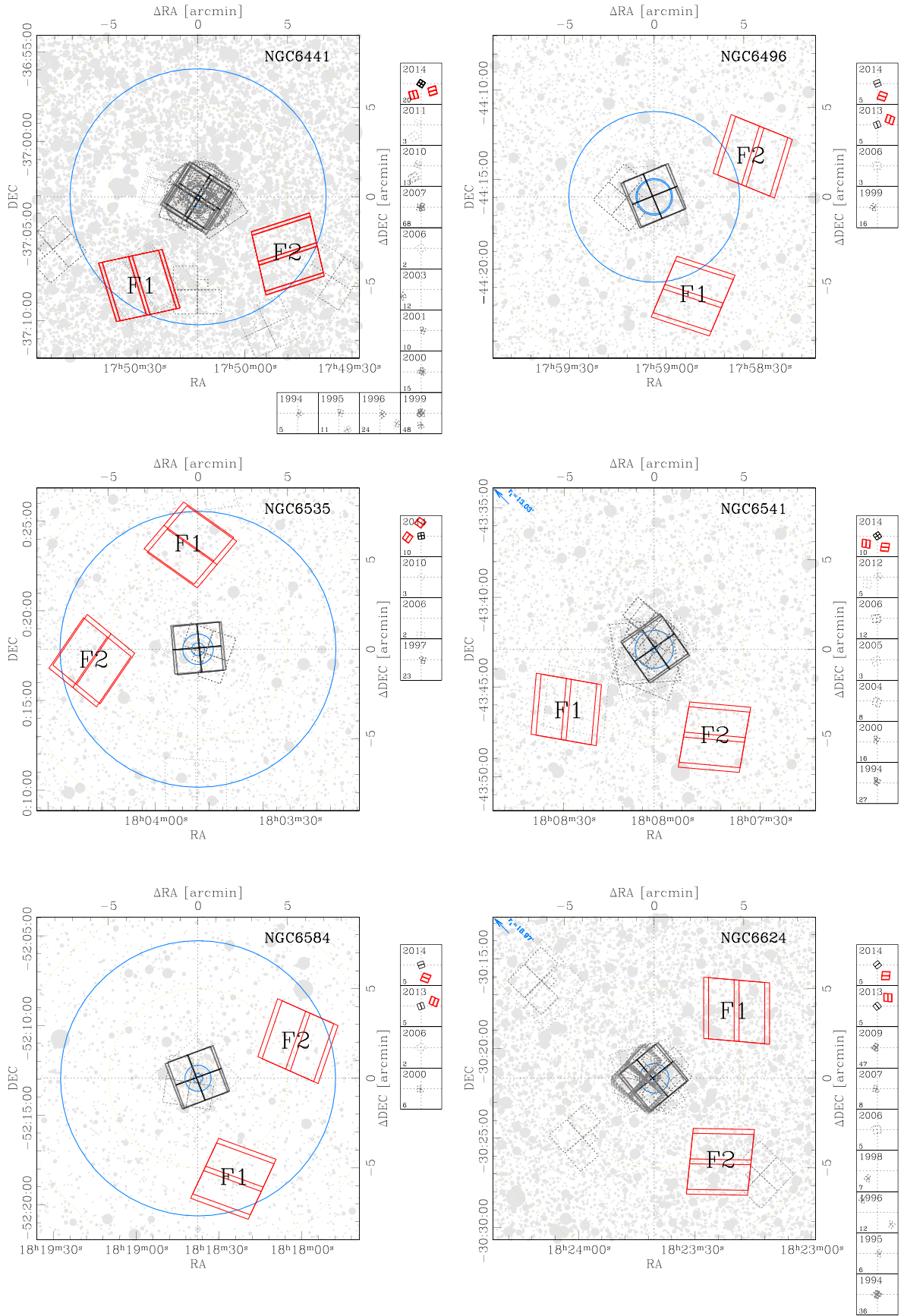


Figure A5. As in Fig. 1 but for NGC 6441, NGC 6496, NGC 6535, NGC 6541, NGC 6584, and NGC 6624.

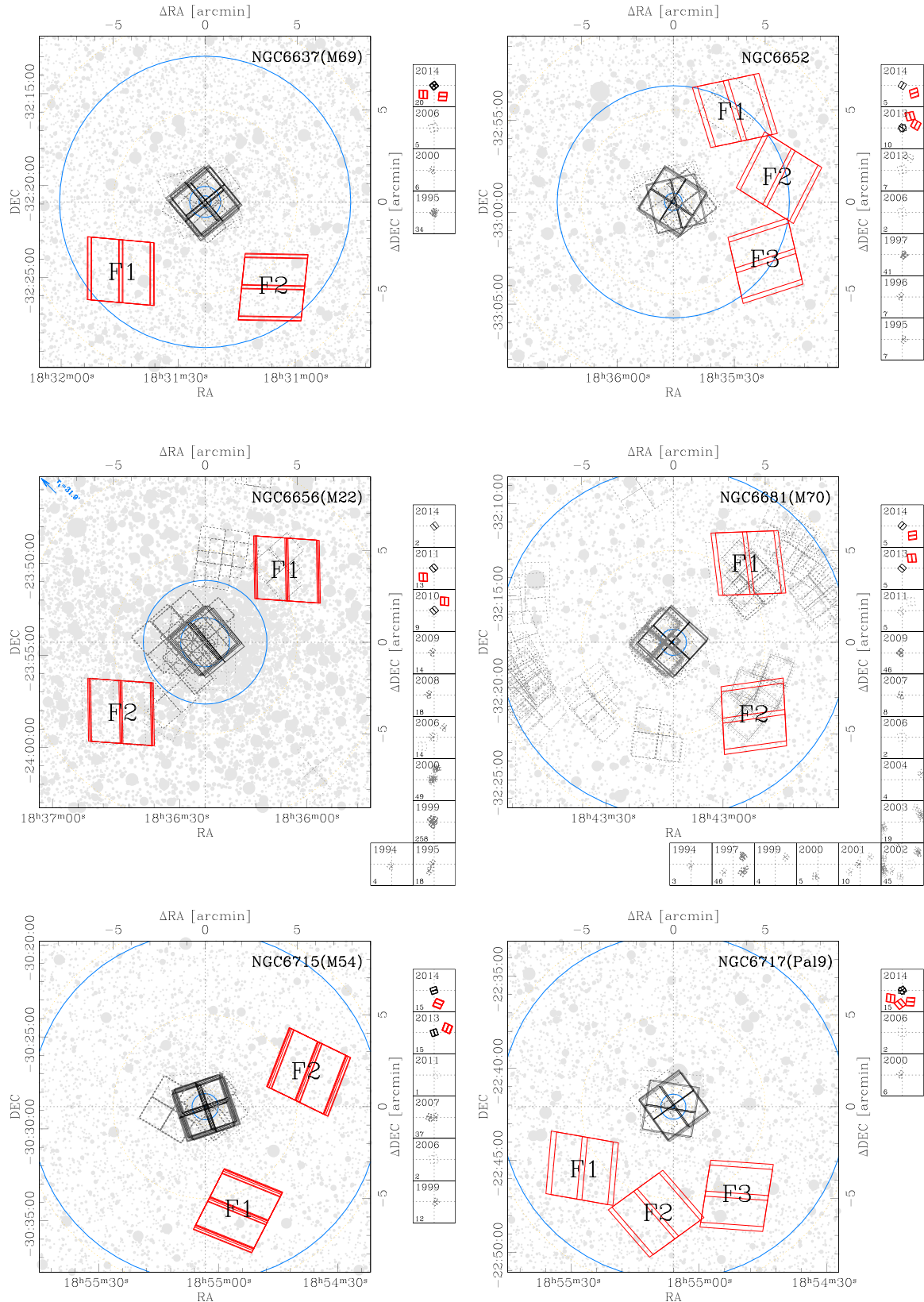


Figure A6. As in Fig. 1 but for NGC 6637, NGC 6652, NGC 6656, NGC 6681, NGC 6715, and NGC 6717.

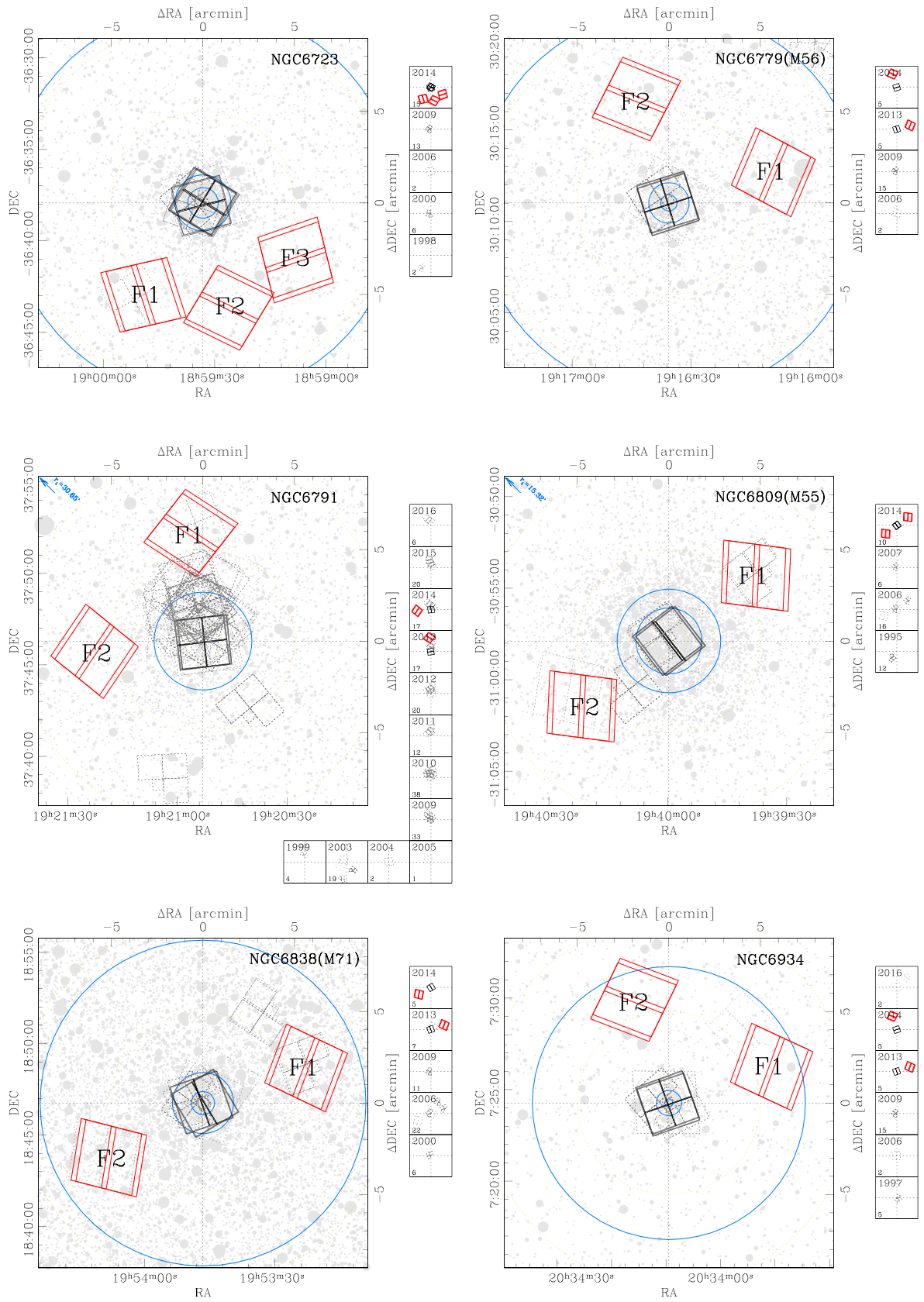


Figure A7. As in Fig. 1 but for NGC 6723, NGC 6779, NGC 6791, NGC 6809, NGC 6838, and NGC 6934.

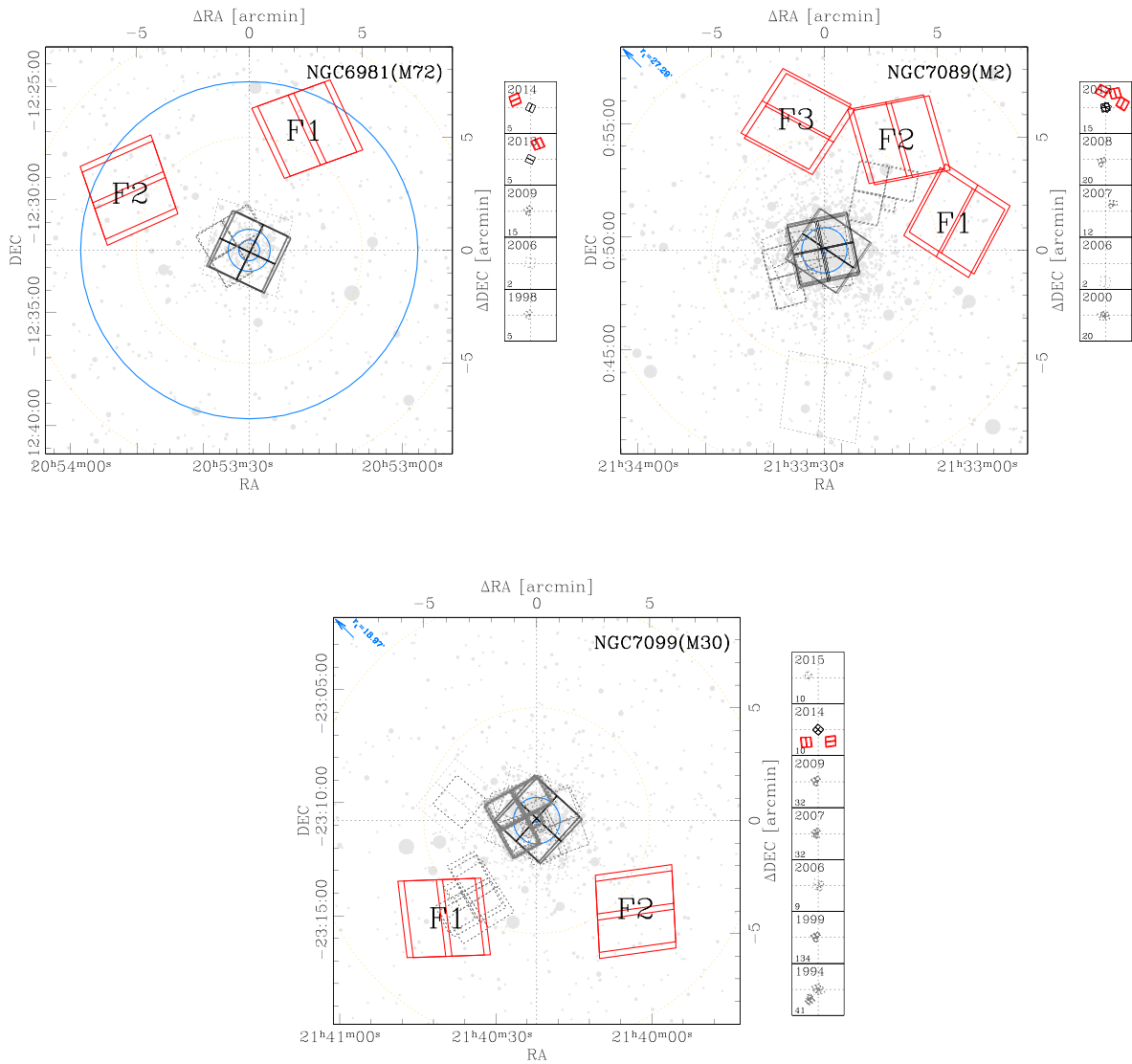


Figure A8. As in Fig. 1 but for NGC 6981, NGC 7089, and NGC 7099.

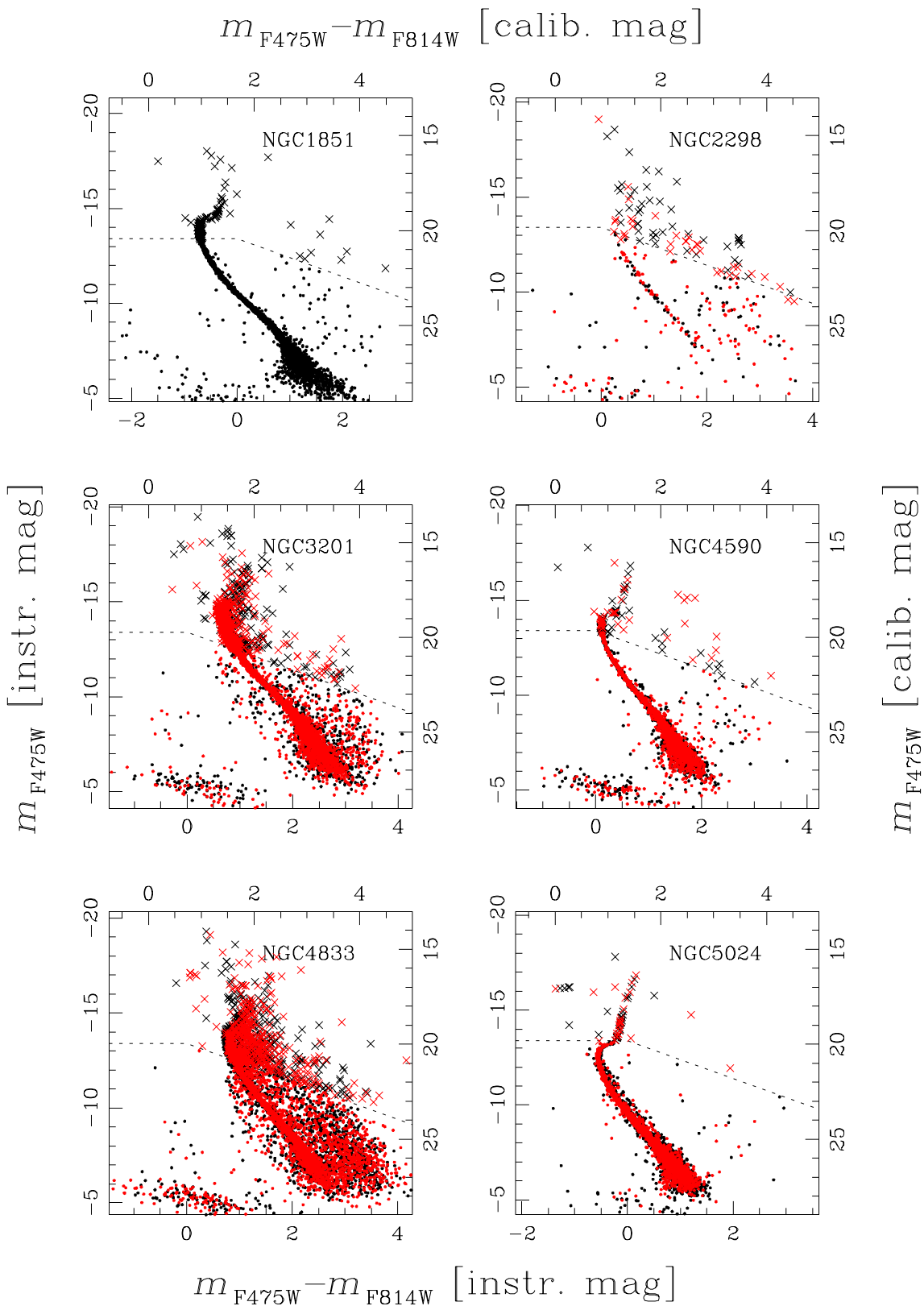


Figure A9. Obtained CMDs for NGC 1851, NGC 2298, NGC 3201, NGC 4590, and NGC 5024. For each cluster, CMDs for all fields have been merged together. The colour-code is such that black dots represent stars measured in F1; red dots, stars of F2; green dots stars of F3; blue dots stars of F4 and orange dots represent stars measured in F5. Dashed lines represent the saturation level for all F1, saturated stars are represented by crosses.

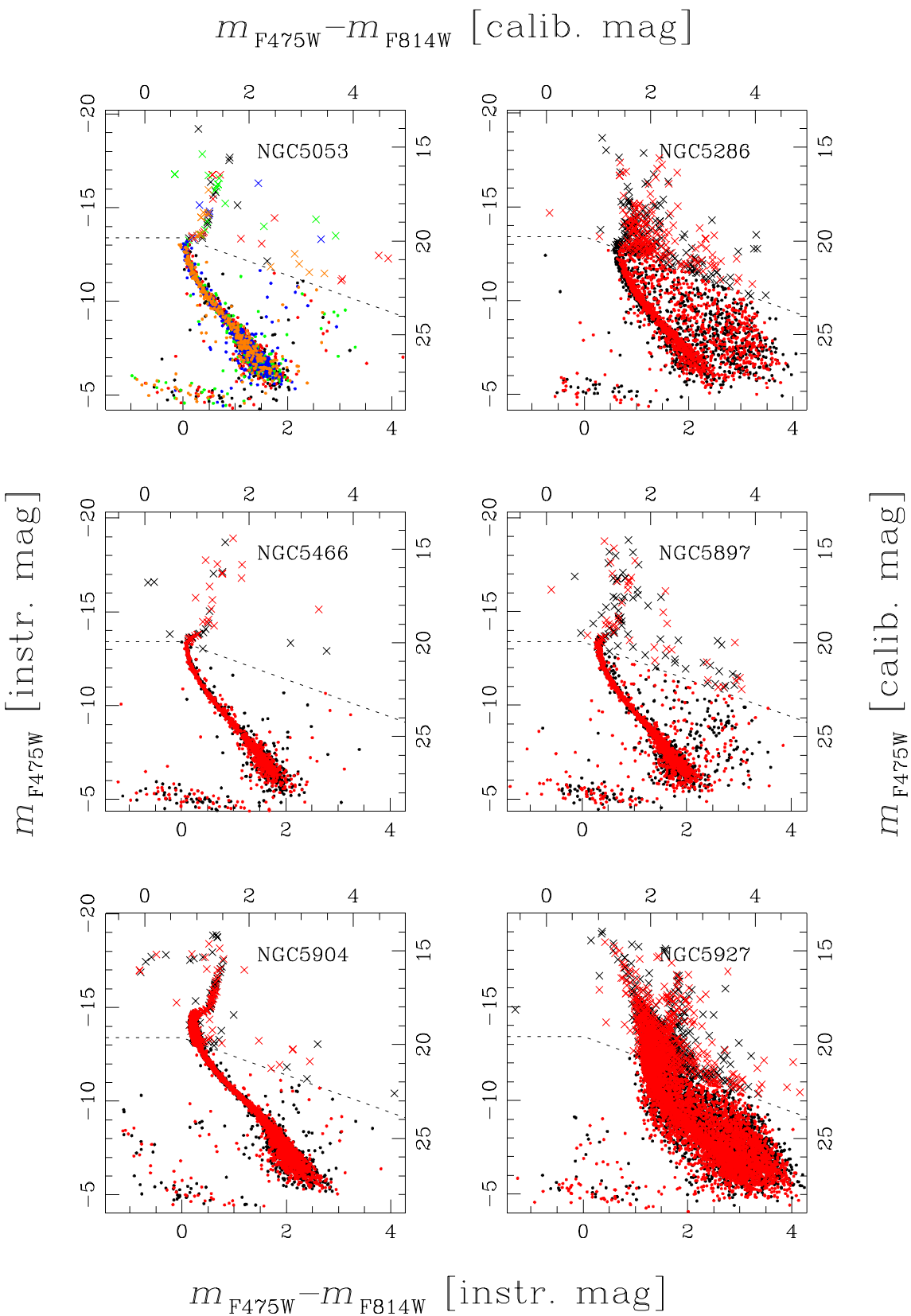


Figure A10. As in Fig. A9 but for NGC 5053, NGC 5286, NGC 5466, NGC 5897, NGC 5904, and NGC 5927.

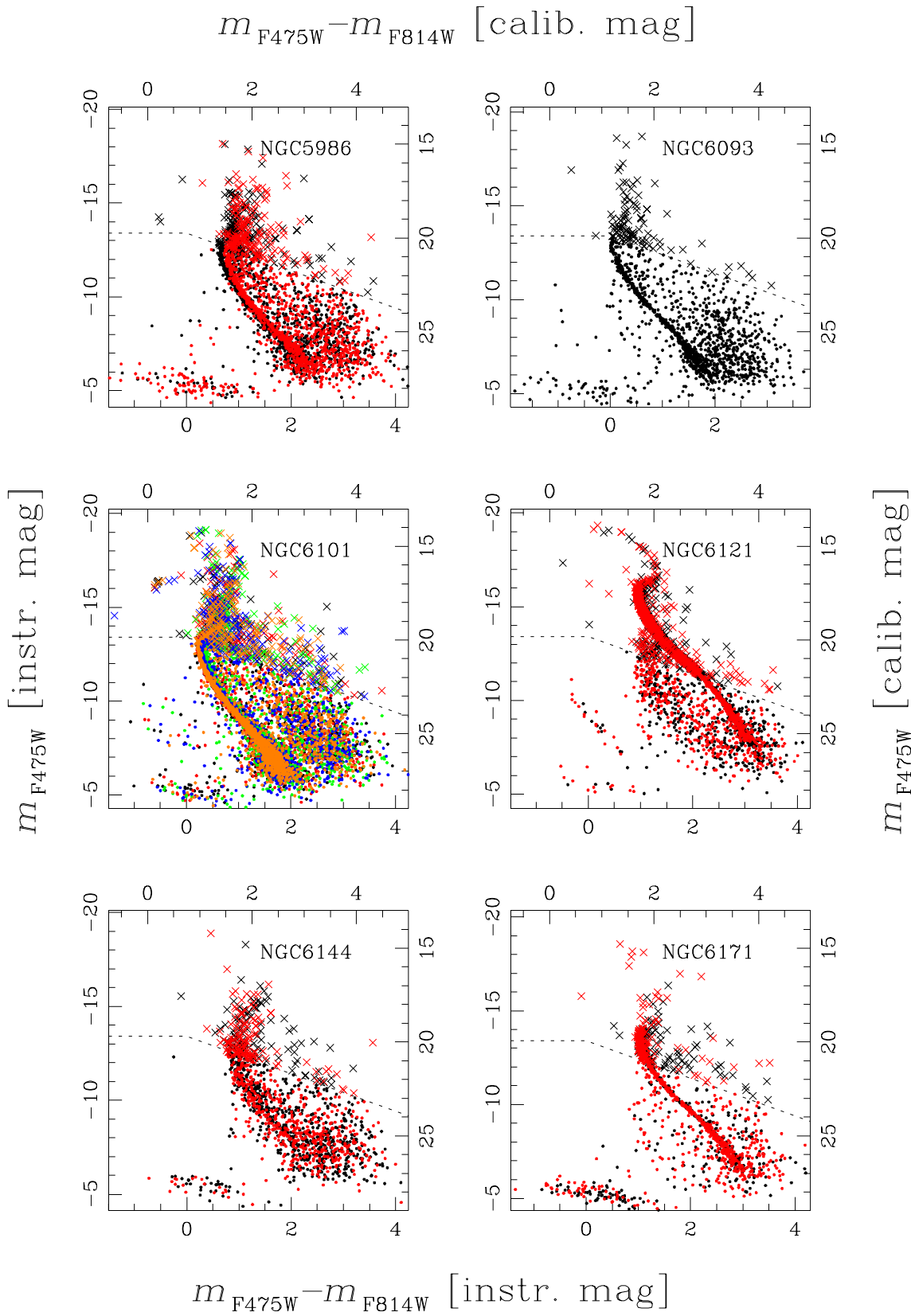


Figure A11. As in Fig. A9 but for NGC5986, NGC6093, NGC6101, NGC6121, NGC6144, and NGC6171.

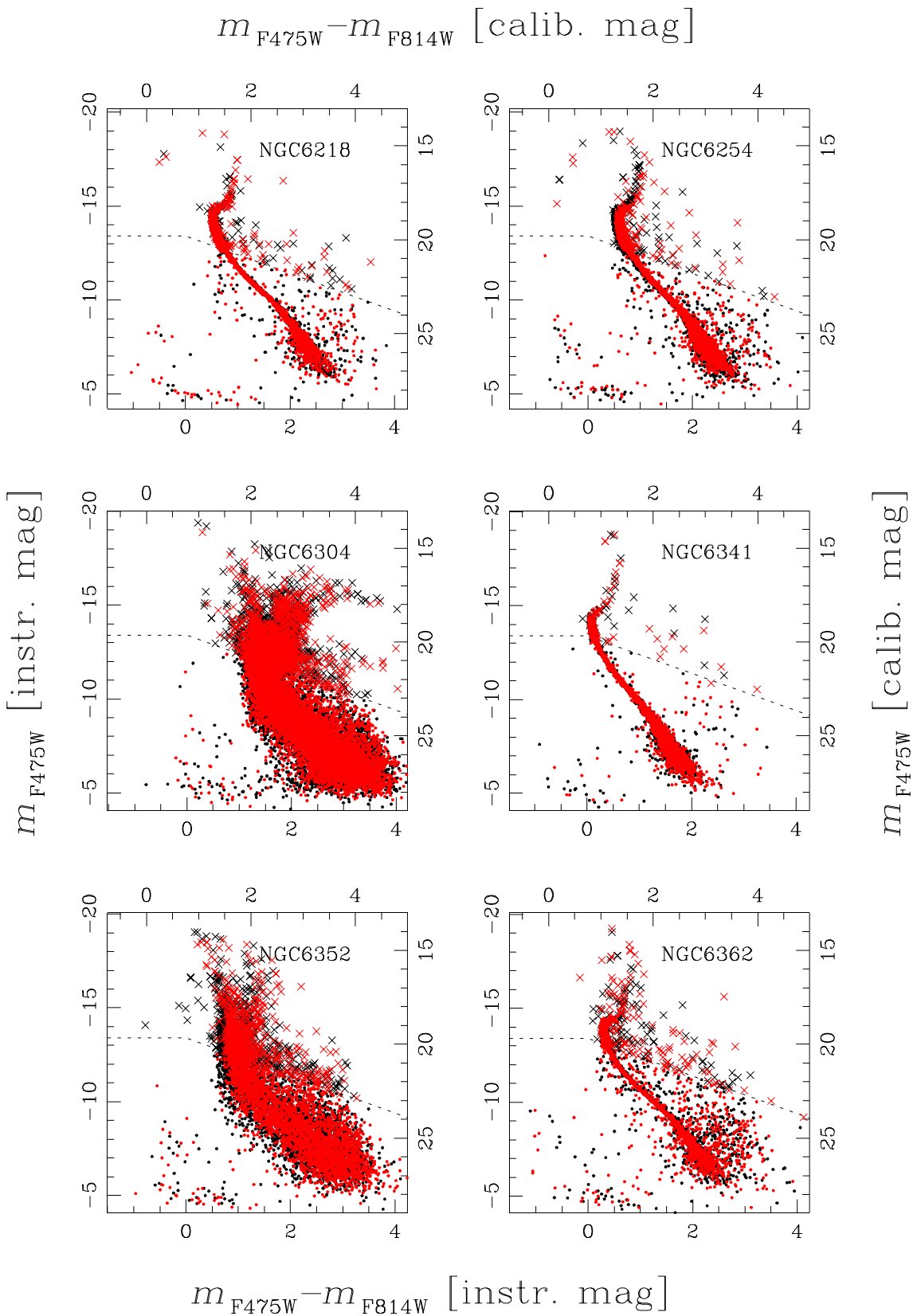


Figure A12. As in Fig. A9 but for NGC 6218, NGC 6254, NGC 6304, NGC 6341, NGC 6352, and NGC 6362.

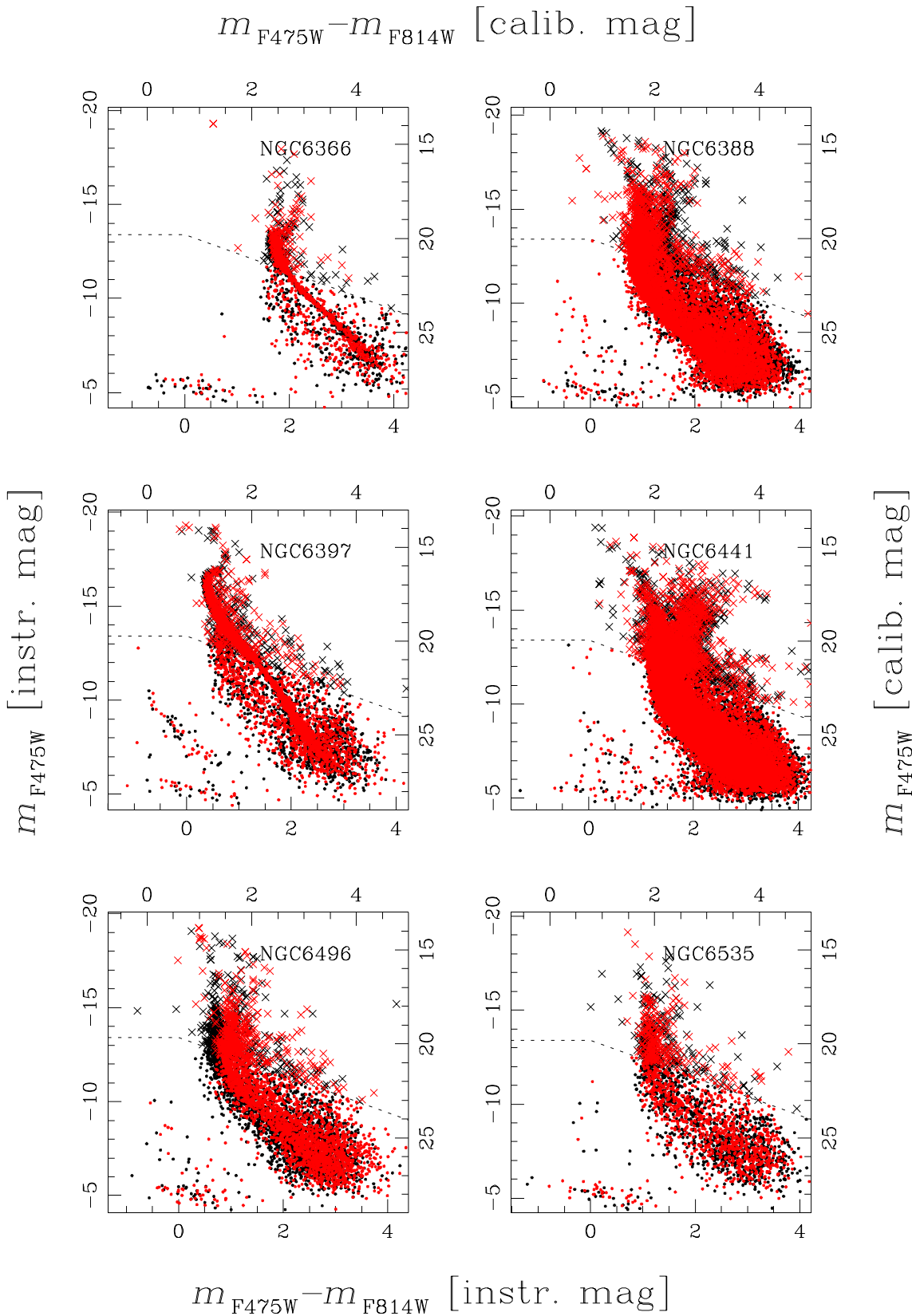


Figure A13. As in Fig. A9 but for NGC 6366, NGC 6388, NGC 6397, NGC 6441, NGC 6496, and NGC 6535.

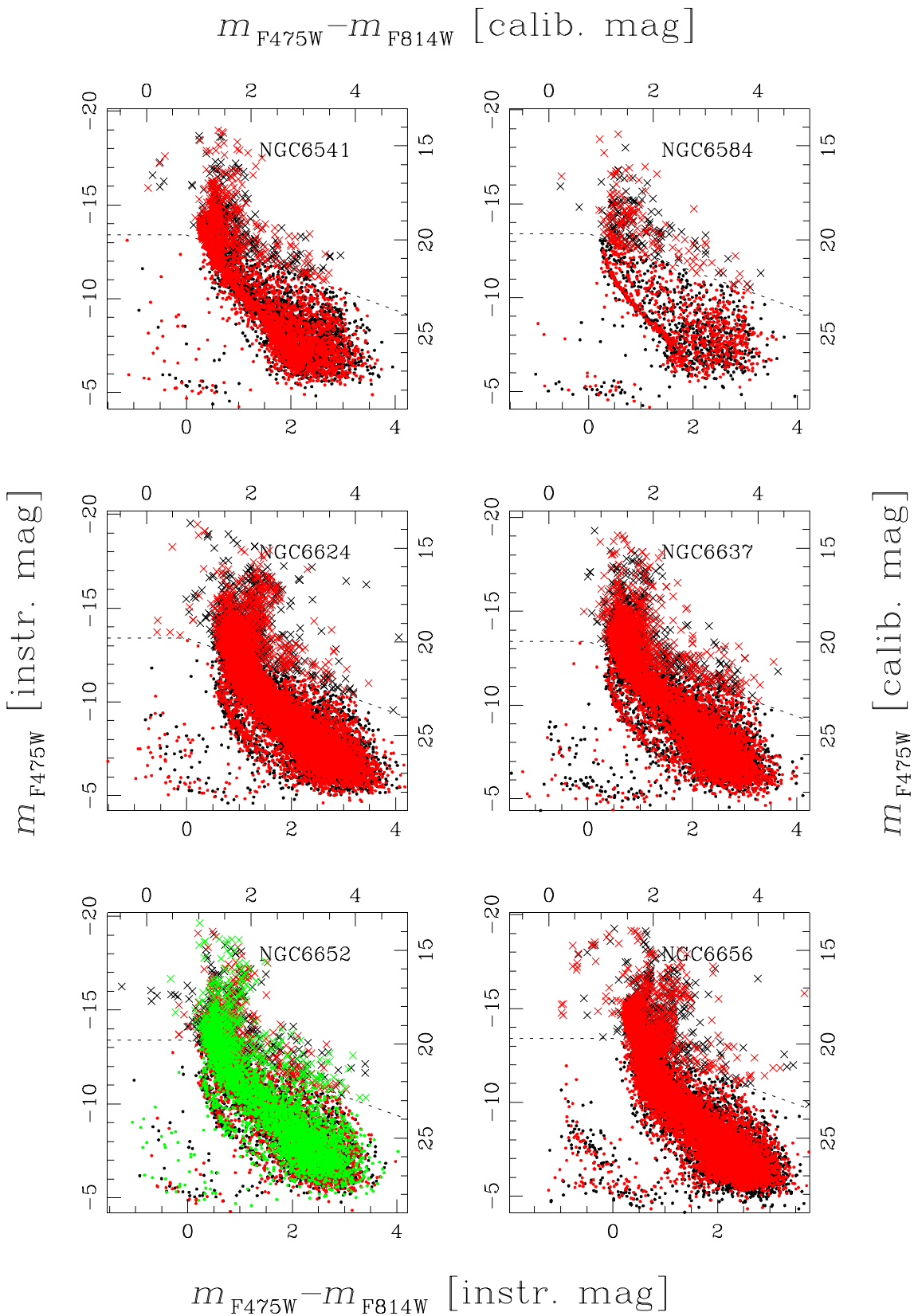


Figure A14. As in Fig. A9 but for NGC 6541, NGC 6584, NGC 6624, NGC 6637, NGC 6652, and NGC 6656.

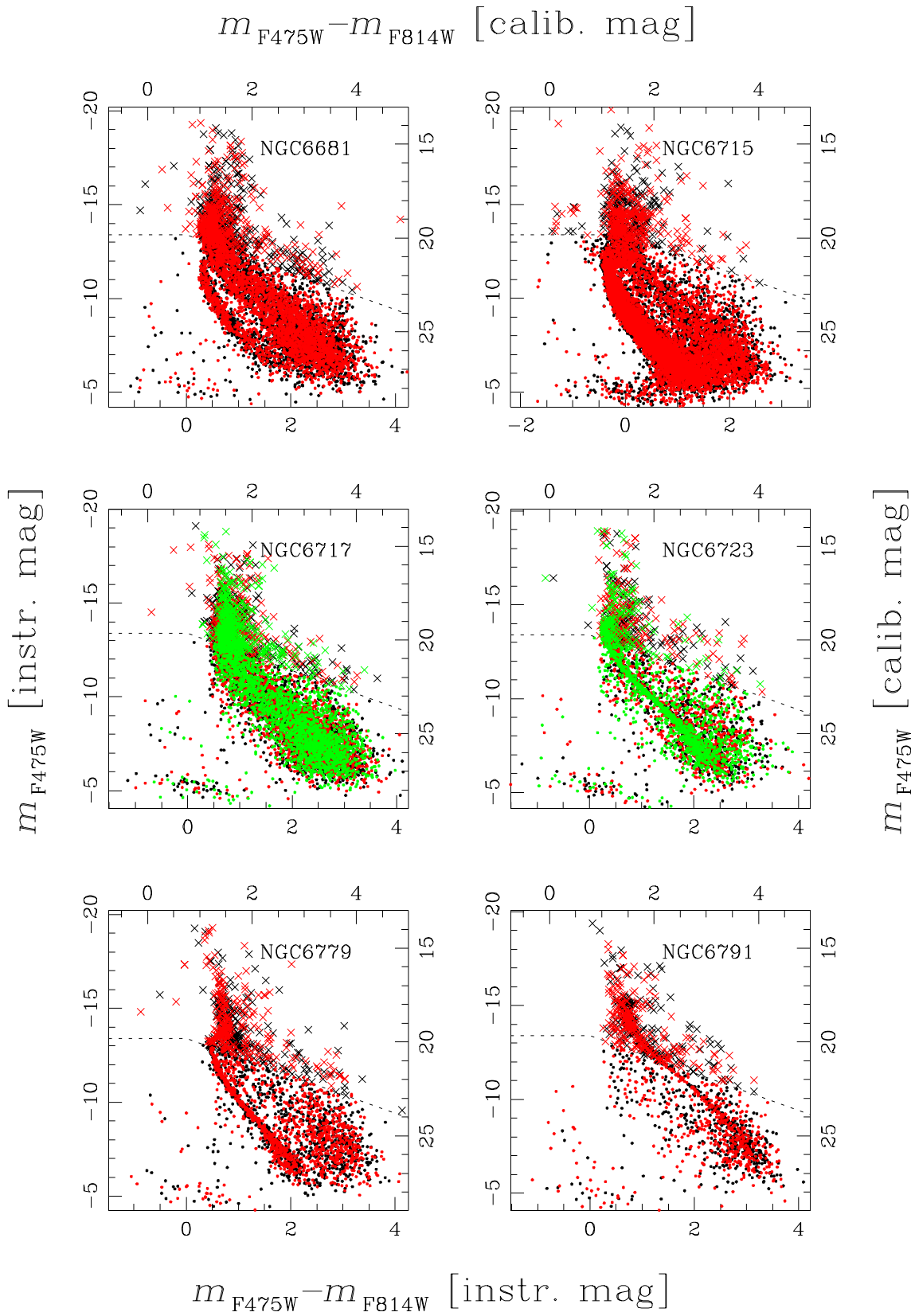


Figure A15. As in Fig. A9 but for NGC 6681, NGC 6715, NGC 6717, NGC 6723, NGC 6779 and NGC 6791.

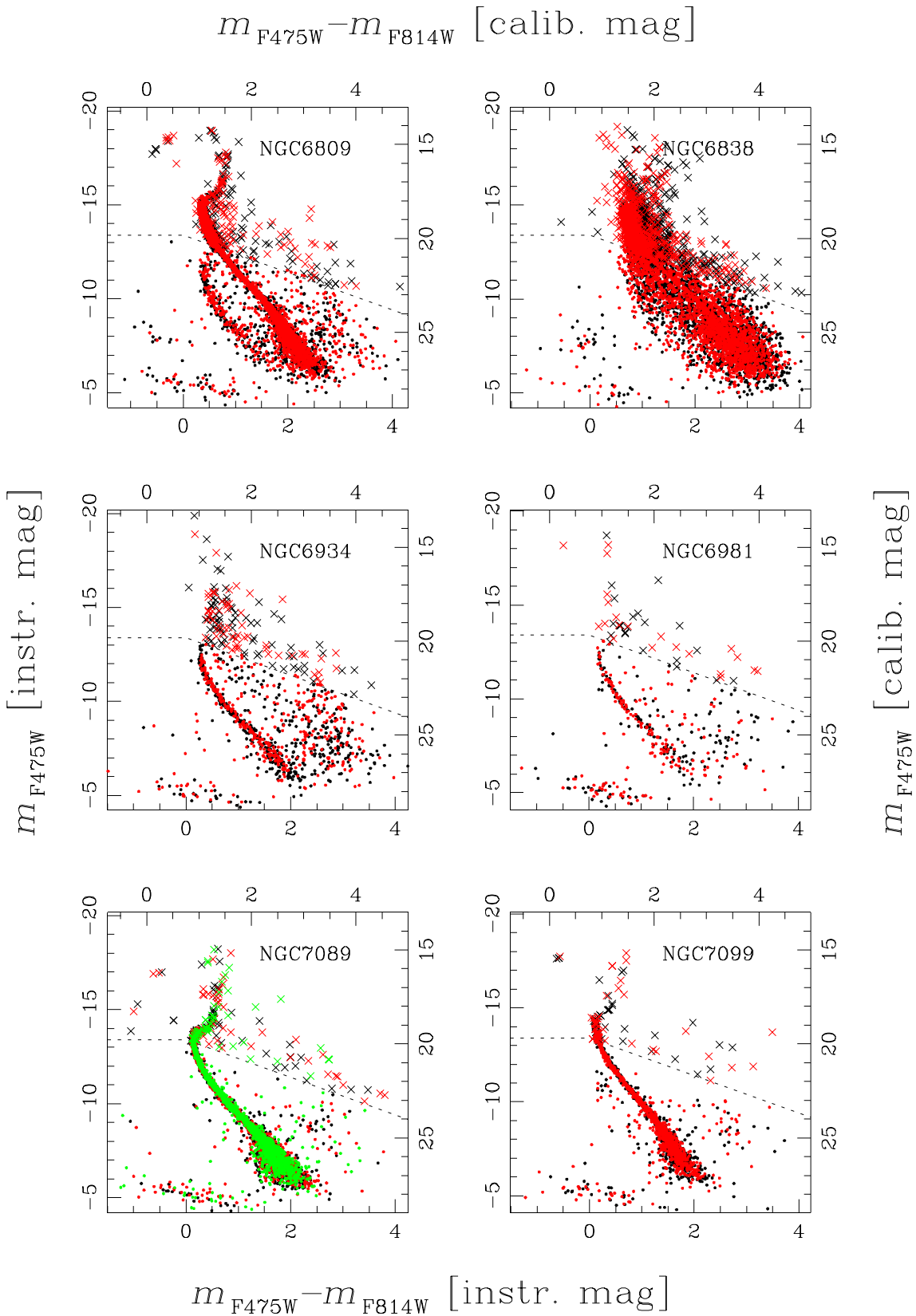


Figure A16. As in Fig. A9 but for NGC 6809, NGC 6838, NGC 6934, NGC 6981, NGC 7089, and NGC 7099.